International Journal of Modern Physics A

D HADRONIC DECAYS AT CLEO-c

FAN YANG
Fermi National Accelerator Laboratory,
Batavia, Illinois 60510, USA
yangf@fnal.gov

Received September 14, 2011
Revised September 14, 2011

The recent CLEO-c results on hadronic decays of D and D_s mesons are presented. First the absolute branching fractions for D and D_s mesons using a double tag technique are discussed, then are the Cabibbo suppressed decays and doubly Cabibbo suppressed decays. Finally, I present the inclusive and rare decay modes and other measurements from CLEO-c. These decays illuminate a wide range of physics. A brief theoretical introduction is given before the corresponding discussion on measurement.

Keywords: D and D_s mesons; hadronic decays; charm.

PACS numbers: 13.25.Ft

1. Introduction

The discovery of charmed meson states signaled a new era in particle physics. The arrival of the first heavy quark has solidified the evidence that the standard model (SM) provides a correct low-energy description of particle physics. In November 1974, the J/ψ resonance was experimentally discovered by two independent research groups at BNL [1] and SLAC [2]. The mass of the observed J/ψ resonance of about 3.1 GeV/c^2 was in the range where a $c\bar{c}$ bound state was expected. The interpretation of J/ψ as a $c\bar{c}$ bound state was confirmed when "open charm" states were discovered a little later, first the D^0 [3] and then the D^+ [4]. There were several candidates observed before the D_s^+, originally called the F meson, was observed by CLEO [5] .

The lightest "open charm" mesons (the D^0, D^+, and D_s^+) decay through the weak interaction, and the majority of their decays are to final states containing only hadrons. Hadronic decays of the stable "open charm" mesons are interesting for several reasons. Absolute measurements of charm meson branching fractions affect our knowledge of several D and B meson decays, from which Cabibbo-Kobayashi-Maskawa (CKM) parameters are extracted. The studies of two- and three-body D decay amplitudes shed light on how long distance hadronic physics affects the visible results of short-distance weak processes. Nonleptonic decays of charmed hadrons provide information [6] that can help in determinations of CKM angles β [7] and γ [8]

in B decays as well as in the determination of $D^0 - \bar{D}^0$ mixing parameters without explicit knowledge of hadronic strong phases [7–9]. These D and D_s mesons and their hadronic decays lie at an intersection of weak and strong physics: the easiest detection of charmed states for flavor physics is through hadronic decays with large rates and simple topologies, while the decay processes themselves provide important information on hadronic spectroscopy and strong interactions. More general overviews of hadronic D and D_s meson decays are given in Ref. 10–12.

In this review we summarise recent results in nonleptonic branching fraction measurements of D^0, D^+ and D_s^+ mesons from CLEO-c experiment, including measurements of absolute and relative branching fractions in exclusive and inclusive modes, and measurements of direct CP violation.

2. The CLEO-c Detector

CLEO-c open charm data was produced by the Cornell Electron Storage Ring (CESR), a symmetric e^+e^- collider, taken with the general-purpose solenoidal detector. The CLEO-c detector is an evolution of the CLEO III detector [13–15] in which the silicon-strip vertex detector has been replaced with a six-layer vertex drift chamber, whose wires are all at small stereo angles to the axis of the chamber. These stereo angles allow hit reconstruction in the demension parallel to the drift chamber axis. The CLEO-c experiment is shown schematically in Fig. 1.

The charged particle tracking system covers a solid angle of 93% of 4π and consists of a small-radius, six-layer, low-mass, stereo wire drift chamber, concentric with, and surrounded by, a 47-layer cylindrical central drift chamber. The chambers operate in a 1.0 T magnetic field and achieve a momentum resolution of $\sim$0.6% at p =1 GeV/c.

Photons are detected in an electromagnetic calorimeter consisting of 7800 cesium iodide crystals and covering 95% of 4π. For energies of 1 GeV the calorimeter has an energy resolution of about 2.2%. For energies of 100 MeV the resolution is about 5%. The excellent energy resolution and coverage allow CLEO-c to efficiently reconstruct π^0 and η mesons in the $\gamma\gamma$ final state. The π^0 mass resolution obtained is about 6 MeV/c^2.

CLEO-c utilizes two particle identification (PID) devices to separate charged kaons from pions: the central drift chamber, which provides measurements of ionization energy loss (dE/dx), and, surrounding this drift chamber, a cylindrical ring-imaging Cherenkov (RICH) detector, whose active solid angle is 80% of 4π. The combined PID system has a pion or kaon efficiency $> 85\%$ and a probability of pions faking kaons (or vice versa) $< 5\%$ [16].

The response of the CLEO-c detector is studied with a detailed GEANT-based [17] Monte Carlo (MC) simulation, with initial particle trajectories generated by EvtGen [18] and final state radiation produced by PHOTOS [19]. Simulated events are reconstructed and selected for analysis with the reconstruction programs and selection criteria used for data.

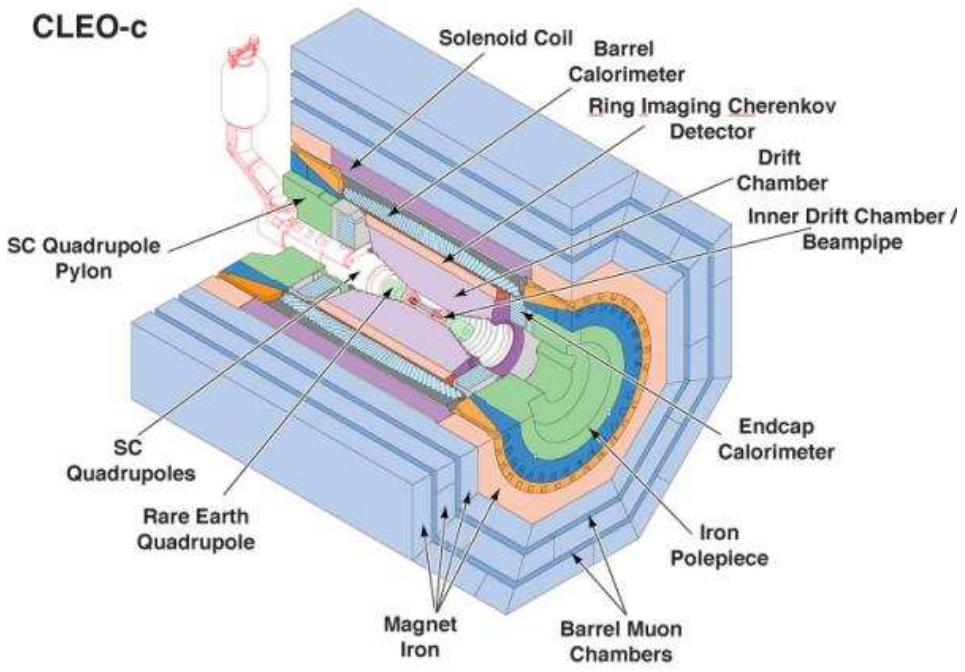

Fig. 1. The CLEO-c detector. The charged particle tracking system consists of an inner drift chamber near the interaction point and the main drift chamber for the momentum measurement. Radially outside the main drift chamber is the CLEO-c RICH detector for charged hadron identification followed by the CsI electromagnetic calorimeter. The instrumented flux return for muon detectors is outside the super conducting solenoid coil. (Figure from reference, see text.)

3. CLEO-c Open Charm Data Samples

3.1. *The $D^0\bar{D}^0$ and D^+D^- sample*

For studies of D^0 and D^+ meson decays, CLEO-c has collected a total integrated luminosity of 818 pb^{-1} of e^+e^- data at the $\psi(3770)$ resonance, the center-of-mass (CM) energy near $E_{\rm cm} = 3774$ MeV, where the cross section for $D\bar{D}$ production is 6 nb [16], and the reaction is $e^+e^- \to D\bar{D}$, with no additional particles. The data sample contains about 2.4×10^6 D^+D^- events (events of interest), 3×10^6 $D^0\bar{D}^0$ events (events of interest), 15×10^6 $e^+e^- \to u\bar{u},\ d\bar{d}$, or $s\bar{s}$ continuum events, 3×10^6 $e^+e^- \to \tau^+\tau^-$ events, and 3×10^6 $e^+e^- \to \gamma\psi'$ radiative return events (sources of background), as well as Bhabha events, μ-pair events, and $\gamma\gamma$ events (useful for luminosity determination and resolution studies).

3.2. *The $D_s^{\pm}D_s^{*\mp}$ sample*

For studies of D_s meson decays, it was less obvious at what center-of-mass energy to run. In order to find a favorable point for studying D_s meson decays, CLEO-c

scanned that region with integrated luminosities of about 5 pb^{-1} per point [20]. The cross sections for producing $D_{(s)}$, or $D^*_{(s)}$ mesons are shown in Fig. 2 [20]. Two possibilities revealed themselves: $E_{\rm cm} = 4010$ MeV, where the cross section for $D_s^+ D_s^-$ production is $(0.269 \pm 0.030 \pm 0.015)$ nb [20], and $E_{\rm cm} = 4170$ MeV, where the cross section for $D_s^{*\pm} D_s^{\mp}$ production is $(0.916 \pm 0.011 \pm 0.049)$ nb [20]. CLEO-c ran at the higher energy of $E_{\rm cm} = 4170$ MeV. At this energy pairs of $D_s^{*\pm} D_s^{\mp}$ mesons are produced. The D_s^* meson decays to either $D_s\gamma$ or $D_s\pi^0$, with branching fractions of $(94.2 \pm 0.7)\%$ and $(5.8 \pm 0.7)\%$ [21,22,23,24], respectively. For most analyses, the advantage of three times larger cross section outweighed the disadvantage of having to cope with the extra complications coming from $D_s^* \to D_s\gamma$ and $D_s^* \to D_s\pi^0$. The data sample consists of an integrated luminosity of 586 pb^{-1} containing about 5.4×10^5 $D_s^{*\pm} D_s^{\mp}$ pairs. Other charm production totals $\sim$7 nb [20], and the underlying light-quark "continuum" is about 12 nb. Through this review, charge conjugate modes are implicitly assumed, unless otherwise noted.

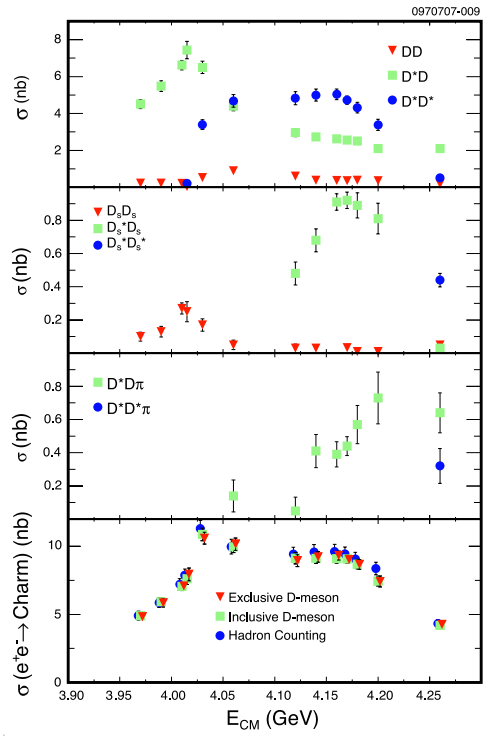

Fig. 2. Exclusive cross sections for two-body and multibody charm meson final states, and total observed charm cross section with combined statistical and systematic uncertainties. (Figure from reference, see text.)

4. Analysis Procedure

At the energies of the $\psi(3770)$ resonance and $E_{\rm cm} = 4170$ MeV, D mesons are produced in pairs without additional hadrons. These unique $D\bar{D}$ final states provide a powerful tool for avoiding the most vexing problem of the difficulty of accurately determining the number of D mesons produced. CLEO-c experiment employs a tag technique pioneered by the MARK III Collaboration [25,26] at SPEAR. Select "single tag" (ST) events in which either a D or $\bar{D}$ is reconstructed without reference to the other particle, and "double tag" (DT) events in which both the D and $\bar{D}$ are reconstructed. These techniques of "single tag" and "double tag" are utilized by most CLEO-c analyses involving D decays [27,28].

4.1. *Final state particles in D meson decays*

The D candidates are built from charged kaons and pions, π^0, η, η' and K^0_S mesons. Many analyses [29,30,31] at CLEO-c make use of fully reconstructed D candidates. The common selection requirements for final state particles used in the reconstruction of D candidate are described in detail elsewhere [16].

Charged tracks produced in the D decay are required to satisfy criteria based on the track fit quality, and the polar angles θ with respect to the beam line, satisfying $|\cos\theta| < 0.93$. Momenta of charged particles utilized in D^0 and D^+ candidate reconstructions must be above 50 MeV/c, while those for D_s must be above 100 MeV/c to eliminate the soft pions from $D^*\bar{D}^*$ and $D^*\bar{D}$ decays (through $D^* \to \pi D$). Track candidates must also be consistent with their coming from the interaction point in three dimensions. Pion and kaon candidates are required to have dE/dx measurements within three standard deviations (3σ) of the expected value. For tracks with momenta greater than 700 MeV/c, RICH information, if available, is combined with dE/dx.

The π^0 candidates are identified via $\pi^0 \to \gamma\gamma$, detecting the photons in the CsI calorimeter. To avoid having both photons in a region of poorer energy resolution, it is required that at least one of the photons be in the "good barrel" region, $|\cos\theta_\gamma| < 0.80$. CLEO-c requires that a calorimeter cluster has a measured energy above 30 MeV, has a lateral distribution consistent with that from photons, and not be matched to any charged track. The invariant mass of the photon pair is required to be within 3σ ($\sigma \sim 6$ MeV/c^2) of the known π^0 mass. A π^0 mass constraint is imposed when π^0 candidates are used in further reconstruction.

The η candidates are reconstructed in two decay modes. For the decay $\eta \to \gamma\gamma$, candidates are formed using a similar procedure as for π^0 except that $\sigma \sim 12$ MeV/c^2. For $\eta \to \pi^+\pi^-\pi^0$, it is required that the invariant mass of the three pions be within 10 MeV of the known η mass [23]. For this decay mode, CLEO-c did not impose a mass constraint. CLEO-c reconstructs η' candidates in the decay mode $\eta' \to \pi^+\pi^-\eta$ and requires $|m_{\pi^+\pi^-\eta} - m_{\eta'}| < 10$ MeV/c^2.

The K^0_S candidates are selected from pairs of oppositely charged and vertex-constrained tracks having invariant mass within 7.5 MeV/c^2, or roughly 3σ, of the

known K^0_S mass [23].

4.2. *Kinematic variables for D^0 and D^+ Candidates*

The $\psi(3770)$ resonance is below the kinematic threshold for $D\bar{D}\pi$ production, so the events of interest, $e^+e^- \to \psi(3770) \to D\bar{D}$, have D mesons with energy equal to the beam energy. Two variables reflecting energy and momentum conservation are used to identify valid D candidates. They are

$$\Delta E \equiv \sum_i E_i - E_{\rm beam},$$

and

$$M_{\rm bc} \equiv \sqrt{E^2_{\rm beam} - (\sum_i \mathbf{p}_i)^2},$$

where $E_i,\ \mathbf{p}_i$ are the energy and momentum of the decay products of a D candidate. For a correct combination of particles, ΔE will be consistent with zero, and the beam-constrained mass $M_{\rm bc}$ will be consistent with the D mass. Candidates are rejected if they fail mode-dependent ΔE requirements. If there is more than one candidate in a particular D or $\bar{D}$ decay mode, CLEO-c usually chooses the candidate with the smallest $|\Delta E|$.

4.3. *Kinematic variables for D^+_s Candidates*

Unlike $D\bar{D}$ threshold events, conventional ΔE and $M_{\rm bc}$ variables are no longer good variables for D_s from $D^{*+}_s D^-_s$ decays, as the D_s can either be a primary or secondary (from a D^*_s decay), with different momentum. The reconstructed invariant mass of the D_s candidate,

$$M(D_s) \equiv \sqrt{(\sum_i E_i)^2 - (\sum_i \mathbf{p}_i)^2},$$

and the mass recoiling against the D_s candidate,

$$M_{\rm recoil}(D_s) \equiv \sqrt{(E_0 - E_{D_s})^2 - (\mathbf{p}_0 - \mathbf{p}_{D_s})^2},$$

are used as primary kinematic variables to select a D_s candidate. Here $E_i,\ \mathbf{p}_i$ are the energy and momentum of the decay products of a D_s candidate, $(E_0, \mathbf{p}_0)$ is the net four-momentum of the e^+e^- system, taking the finite beam crossing angle into account, $\mathbf{p}_{D_s}$ is the momentum of the D_s candidate, $E_{D_s} = \sqrt{m^2_{D_s} + \mathbf{p}^2_{D_s}}$, and m_{D_s} is the known D_s mass [23]. In the single tag case, CLEO-c made no requirements on the decay of the other D_s in the event.

There are two components in the recoil mass distribution, a peak around the D^*_s mass if the candidate is due to the primary D_s, and a rectangular shaped distribution if the candidate is due to the secondary D_s from a D^*_s decay. The edges of $M_{\rm recoil}(D_s)$ from the secondary D_s are kinematically determined (as a function of

$\sqrt{s}$ and known masses), and at $\sqrt{s} = 4170$ MeV, $\Delta M_{\rm recoil}(D_s) \equiv M_{\rm recoil}(D_s) - m_{D_s^*}$ is in the range $[-54, 57]$ MeV/c^2. Initial state radiation (ISR) causes a tail on the high side, above 57 MeV/c^2. At CLEO-c, usually the D_s candidates are selected within the -55 MeV/$c^2 \leq \Delta M_{\rm recoil}(D_s) < +55$ MeV/c^2 range. This window allows both primary and secondary D_s candidates to be selected.

Some of CLEO-c analyses [28,29,30,31] require a photon consistent with coming from $D_s^{*+} \to D_s^+\gamma$ decay, by looking at the mass recoiling against the D_s candidate plus γ system,

$$M_{\rm recoil}(D_s\gamma) \equiv \sqrt{(E_0 - E_{D_s} - E_\gamma)^2 - (\mathbf{p}_0 - \mathbf{p}_{D_s} - \mathbf{p}_\gamma)^2}.$$

For correct combinations, this recoil mass peaks at m_{D_s}, regardless of whether the candidate is due to a primary or a secondary D_s. The typical CLEO-c requirement on this recoil mass is $|M_{\rm recoil}(D_s\gamma) - m_{D_s}| < 30$ MeV/c^2. This requirement improves the signal to noise ratio, important for the suppressed modes. Every event is allowed to contribute a maximum of one D_s candidate per mode and charge. If there are multiple candidates, the one with $M_{\rm recoil}(D_s\gamma)$ closest to m_{D_s} is chosen.

5. Theoretical Considerations of D Meson Decays

Hadronic decays of D mesons involve transitions of the initial-state D meson into several final state mesons or baryons. Thus, they are described by an effective Hamiltonian containing four-quark operators. The theoretical description of fully hadronic decays of charm mesons is significantly more complicated than that of leptonic or semileptonic decays, even though relevant effective Hamiltonians appear similar [10,11]. Charmed hadronic decays are usually classified by their degree of Cabibbo-Kobayashi-Maskawa (CKM) matrix element suppression.

5.1. *Cabibbo favored decays*

The least suppressed of these decays, where the quark level transitions are $c \to su\bar{d}$, are labeled "Cabibbo favored" (CF) decays and governed [10,11] by

$$\begin{aligned} \mathcal{H}_{CF} &= \frac{G_F}{\sqrt{2}} V_{ud} V_{cs}^* \left[C_1(\mu)\mathcal{O}_1 + C_2(\mu)\mathcal{O}_2 \right] + \text{h.c}, \\ \mathcal{O}_1 &= (\overline{s}_i \Gamma_\mu c_i)\,(\overline{u}_k \Gamma^\mu d_k)\,, \qquad \mathcal{O}_2 = (\overline{s}_i \Gamma_\mu c_k)\,(\overline{u}_k \Gamma^\mu d_i)\,, \end{aligned} \tag{1}$$

where $C_n(\mu)$ are the Wilson coefficients obtained by perturbative QCD running from M_W scale to the scale μ relevant for hadronic decay, and the Latin indices denote quark color. G_F is a Fermi constant, and $\Gamma_\mu = \gamma_\mu\,(1 - \gamma_5)$.

5.2. *Cabibbo suppressed decays*

The "Cabibbo suppressed" (CS) transitions are driven by $c \to du\bar{d}$ or $c \to su\bar{s}$ quark processes. Due to the presence of the quark-antiquark pair of the same flavor

in the final state, the effective Hamiltonian takes a much more elaborate form [10,11],

$$\begin{aligned}\mathcal{H}_{CS} &= \frac{G_F}{\sqrt{2}} \sum_{q=s,d} V_{uq} V_{cq}^* \left[C_1(\mu) \mathcal{O}_1^q + C_2(\mu) \mathcal{O}_2^q \right] \\ &- \frac{G_F}{\sqrt{2}} V_{ub} V_{cb}^* \sum_{n=3}^{6} C_n(\mu) \mathcal{O} + \text{h.c}, \\ \mathcal{O}_1 &= \left(\overline{q}_i \Gamma_\mu c_i \right) \left(\overline{u}_k \Gamma^\mu q_k \right), \quad \mathcal{O}_2 = \left(\overline{q}_i \Gamma_\mu c_k \right) \left(\overline{u}_k \Gamma^\mu q_i \right), \end{aligned} \tag{2}$$

where $q = d,\ s$, and $\mathcal{O}_{3-6}$ are the so-called "penguin" operators of the type $(\overline{u}c)_{V-A} \sum_q (\overline{q}q)_{V\pm A}$ (see, e.g. Ref. 32). It is often easy to denote the degree of suppression by powers of the Wolfenstein parameter $\lambda = \sin\theta_C = V_{us} \simeq 0.22$, there θ_C is a Cabibbo angle.

The "Doubly Cabibbo suppressed" (DCS) decay is the one in which the $c \to du\bar{s}$ quark transition drives the decay. The effective Hamiltonian for the DCS decay can be obtained from Eq. (1) by interchanging s and d.

5.3. *Approaches for studying hadronic charm decays*

Calculations of hadronic decay rates governed by these transitions are quite complicated and model dependent. Most often, simplified assumptions, such as factorization [33,34] are used to estimate the needed branching ratios. Some dynamical approaches, such as QCD sum rules, have been used to justify those assumptions [35]. Charmed mesons populate the energy range in which non-perturbative quark dynamics is active, leading to resonance effects that affect the phases of hadronic decay amplitudes [36], which makes predictions based on factorization quite unreliable. Finally, standard methods of flavor $SU(3)$ [37] symmetries can be used in studies of hadronic D meson decays.

The relations among several decay rates can be built based on standard flavor $SU(3)$ [37] symmetries or on overcomplete set of universal quark-level amplitudes [38,39]. The partial width for a specific two-body decay of a charmed meson depends on both the invariant amplitude $\mathcal{A}$ and a phase space factor. For a specific two-body decay into a PP final state,

$$\Gamma(D \to PP) = \frac{\mid \mathbf{p} \mid}{8\pi M_D^2} \left| \mathcal{A}(D \to PP) \right|^2, \tag{3}$$

where $|\mathbf{p}|$ is a center-of-mass 3-momentum of each final state particle. For a decay into a PV final state,

$$\Gamma(D \to PV) = \frac{\mid \mathbf{p} \mid^3}{8\pi M_D^2} \left| \mathcal{A}(D \to PV) \right|^2. \tag{4}$$

Note that in the case of PP final state the final state mesons are in the S-wave, while in the case of PV final state they are in a P-wave. This is why $|\mathcal{A}(D \to PP)|$ has dimension of energy, while $|\mathcal{A}(D \to PV)|$ is dimensionless.

6. Absolute Hadronic Branching Fractions of D^0, D^+ and D_s^+ Mesons

Measurements of absolute hadronic D meson branching fractions play a central role in the study of the weak interaction because they serve to normalize many important D meson and hence B meson branching fractions. For example, the determination of $|V_{cb}|$ from $B \to D^* \ell \nu$ [40] depends directly on the determination of the D branching fractions used to reconstruct the final state. Uncertainties in the absolute D_s^+ meson hadronic branching fractions significantly impact the precision of some important measurements, such as tests of the standard model prediction of the coupling of the Z^0 boson to charm quarks, measurements of B meson properties such as B_s^0 mixing parameters, and tests of light quark $SU(3)$ symmetry in D system.

6.1. *Double tag technique*

For the precision measurements of benchmark branching fractions, CLEO-c has used the "double tag" technique pioneered by Mark III [25,26]. In this technique the yields of single tags, where one D meson is reconstructed, and double tags, where both D mesons are reconstructed, are determined. The number of reconstructed single tags, separately for D and $\bar{D}$ decays, are given by

$$N_i = \epsilon_i \mathcal{B}_i N_{D\bar{D}}$$

and

$$\bar{N}_j = \bar{\epsilon}_j \mathcal{B}_j N_{D\bar{D}},$$

respectively, where ϵ_i and $\mathcal{B}_i$ are the efficiency and branching fraction for mode i and $N_{D\bar{D}}$ is the number of produced $D\bar{D}$ pairs. Though the yields are determined separately for D and $\bar{D}$ decays, if CP violation is negligible, then it is assumed that the branching fractions are the same. Similarly, the number of double tags reconstructed is given by

$$N_{ij} = \epsilon_{ij} \mathcal{B}_i \mathcal{B}_j N_{D\bar{D}}$$

where i and j label the D and $\bar{D}$ mode used to reconstruct the event and ϵ_{ij} is the efficiency for reconstructing the final state. Combining the two equations above and solving for $N_{D\bar{D}}$ gives the number of produced $D\bar{D}$ events as

$$N_{D\bar{D}} = \frac{N_i \bar{N}_j}{N_{ij}} \frac{\epsilon_{ij}}{\epsilon_i \bar{\epsilon}_j}$$

and the branching fractions

$$\mathcal{B}_i = \frac{N_{ij}}{N_j} \frac{\epsilon_j}{\epsilon_{ij}}.$$

Note that many systematic uncertainties cancel in the ratio of efficiencies. This includes for example track finding efficiencies and particle identification that are common to efficiencies in the denominator and numerator. However, systematic

uncertainties from, for example, the determination of the yields do not cancel as they are not correlated. CLEO-c determines all the single tag and double tag yields in data and the efficiencies from Monte Carlo simulations. The branching fractions and $D\bar{D}$ yields are extracted from a combined fit to all measured data yields and efficiencies [16].

6.2. *Absolute D^0 and D^+ hadronic branching fractions*

CLEO-c has performed absolute measurements of the D^0 and D^+ branching fractions for the Cabibbo favored decays $D^0 \to K^-\pi^+$, $D^0 \to K^-\pi^+\pi^0$, $D^0 \to K^-\pi^+\pi^+\pi^-$, $D^+ \to K^-\pi^+\pi^+$, $D^+ \to K^-\pi^+\pi^+\pi^0$, $D^+ \to K^0_S\pi^+$, $D^+ \to K^0_S\pi^+\pi^0$, and $D^+ \to K^0_S\pi^+\pi^+\pi^-$, and for the Cabibbo suppressed decay $D^+ \to K^+K^-\pi^+$ [16]. Two of these branching fractions, $\mathcal{B}(D^0 \to K^-\pi^+)$ and $\mathcal{B}(D^+ \to K^-\pi^+\pi^+)$, are particularly important because most D^0 and D^+ branching fractions are determined from ratios to one of these branching fractions [21,22,23]. As a result, almost all branching fractions in the weak decay of heavy quarks that involve D^0 or D^+ mesons are ultimately tied to one of these two branching fractions, called reference branching fractions. Furthermore, these reference branching fractions are used in many measurements of Cabibbo-Kobayashi-Maskawa (CKM) matrix elements for c and b quark decay.

The early measurement of absolute hadronic branching fractions of D^0 and D^+ meson decays by CLEO-c was published based on an integrated luminosity of 56 pb^{-1} [41]. Later it was updated with 281 pb^{-1} [16].

6.2.1. *Single tag yields*

Particle identification requirements are applied on charged kaons and pions. The π^0 and K^0_S candidates are reconstructed in the $\gamma\gamma$ and $\pi^+\pi^-$ final states, respectively. The tracks used to reconstruct K^0_S were not subjected to the standard track quality or particle identification requirements. The mode dependent selection criteria on ΔE, the candidate energy minus beam energy, for D candidates are set at approximately 3 standard deviations of the resolution.

The single tag (ST) yields in data events are obtained from simultaneous unbinned maximum likelihood fits to the $M_{\rm bc}(D)$ and $M_{\rm bc}(\bar{D})$ distributions for ST D and $\bar{D}$ events separately. These fits are shown in Fig. 3 [16] where the D and $\bar{D}$ decays have been combined. Each fit included a signal line shape function [16] for signal and a modified ARGUS function[42] for the combinatorial background.

For the signal shape CLEO-c has used several different parameterizations. The most detailed description is that used in this measurement [16]. This form incorporates the effects of detector resolution, beam energy distribution, initial state radiation, and the line shape of the $\psi(3770)$. The beam energy distribution, initial state radiation, and the $\psi(3770)$ lineshape control the energy of the produced D mesons. The effect of ISR is to produce the $\psi(3770)$ with an energy below the nominal e^+e^- center-of-mass energy. This produces a tail on the high side of the $M_{\rm bc}$

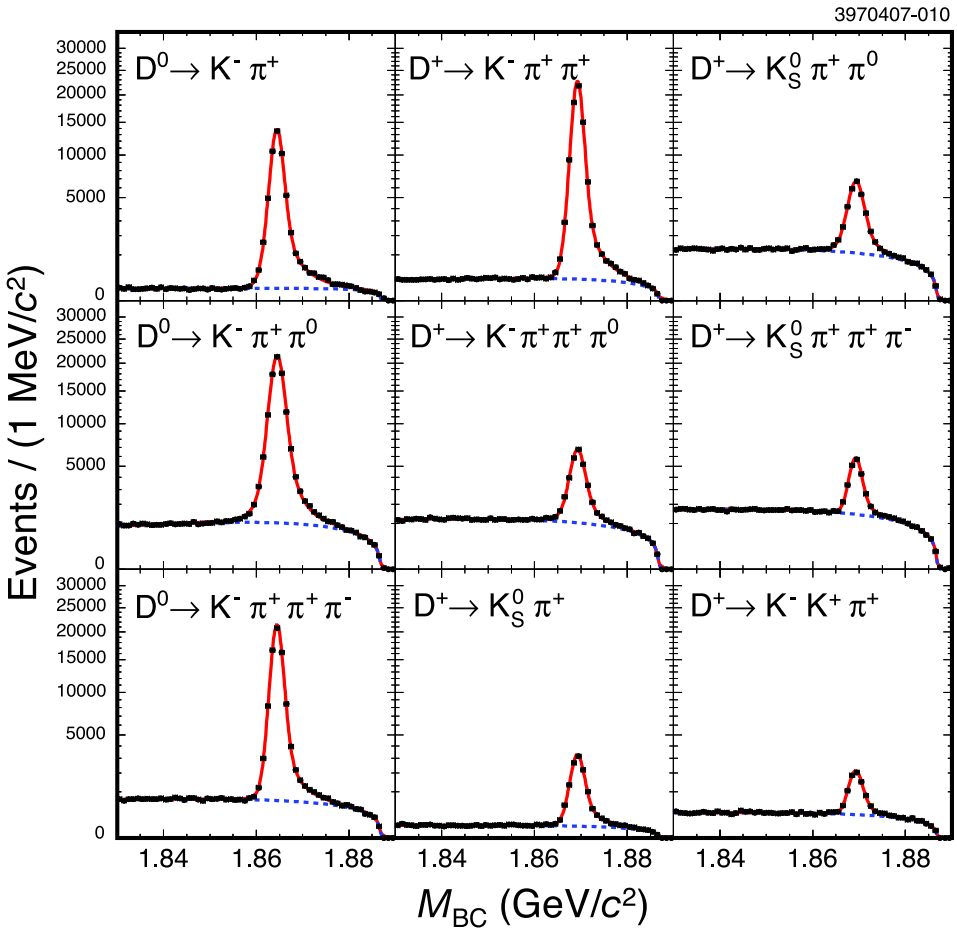

Fig. 3. Distributions of measured $M_{\rm bc}(D)$ or $M_{\rm bc}(\bar{D})$ values for single tag D^0 and D^+ candidates with D and $\bar{D}$ candidates combined in each mode. The points are data and the curves are fits to the data. In each plot, the dashed curve shows the contribution of the ARGUS background function and the solid curve shows the sum of this background and the signal peak function. The number of events in each bin is plotted on a square-root scale. The ST D^0 decays are illustrated in the left column and the ST D^+ decays are illustrated in the other two columns. The reference modes $D^0 \to K^-\pi^+$ and $D^+ \to K^-\pi^+\pi^+$ are illustrated in the first two plots from the left in the top row. (Figure from reference, see text.)

distribution as seen in Fig. 3. The detector resolution effects lead to a smearing of the measured momentum which can be described by a sum of three Gaussian

functions,

$$G(\mathbf{p};\mathbf{q},\sigma_p,f_a,s_a,f_b,s_b) = \frac{1}{(2\pi)^{3/2}\sigma_p^3}\Bigg[(1-f_a-f_b)e^{-(\mathbf{p}-\mathbf{q})^2/(2\sigma_p^2)} + \frac{f_a}{s_a^3}e^{-(\mathbf{p}-\mathbf{q})^2/(2(s_a\sigma_p)^2)} + \frac{f_b}{(s_as_b)^3}e^{-(\mathbf{p}-\mathbf{q})^2/(2(s_as_b\sigma_p)^2)}\Bigg]. \quad (5)$$

Here, $\mathbf{q}$ is the true momentum of the D meson; $\mathbf{p}$ is its reconstructed momentum; σ_p is the width of the core Gaussian; $s_a\sigma_p$ is the width of the second Gaussian; f_a is the fraction of candidates that are smeared with the width of the second Gaussian; $s_as_b\sigma_p$ is the width of a third Gaussian; and f_b is the fraction of candidates that are smeared with the width of the third Gaussian. All values of s_a and s_b determined from fits are greater than 2, so the second Gaussian is significantly wider than the first and the third is significantly wider than the second.

Combinatorial backgrounds were described by a modified ARGUS function [42]

$$a(m;m_0,\xi,\rho) = A\,m\left(1-\frac{m^2}{m_0^2}\right)^{\rho}e^{\xi\left(1-\frac{m^2}{m_0^2}\right)}, \quad (6)$$

where m is the candidate mass ($M_{\rm bc}$), m_0 is the endpoint given by the beam energy, and A is a normalization constant. The modification of the original ARGUS function allows the power parameter, ρ, to differ from the nominal value, $\rho = \frac{1}{2}$. The parameters ξ and ρ were determined in each individual ST fit to data or MC simulations.

6.2.2. *Double tag yields*

The double tag yields are determined separately for the $45 = 3^2(D^0) + 6^2(D^+)$ double tag modes. The same requirements on ΔE that were applied for the single tags are applied to the double tags to ensure that the systematic uncertainty from the selection in single and double tag yields cancels in the ratio for the signal mode. To extract the number of double tag candidates a two-dimensional unbinned maximum likelihood fit is performed in the plane of $M_{\rm bc}(D)$ vs. $M_{\rm bc}(\bar{D})$. This is illustrated in Fig. 4 [16]. There is an obvious signal peak in the region surrounding $M_{\rm bc}(\bar{D}) = M_{\rm bc}(D) = M_{D^0}$. The distribution of the signal candidates in this peak is influenced primarily by beam energy spread, and secondarily by the $\psi(3770)$ resonance shape and detector resolution. In addition, the effects of initial state radiation will spread the signal along the diagonal to larger values of $M_{\rm bc}(\bar{D})$ and $M_{\rm bc}(D)$. If all particles produced in the e^+e^- interaction are used to form the D and $\bar{D}$ candidate, but the particles are either from continuum, or from a $D\bar{D}$ event but not assigned to the right D candidate (mispartitioned $D\bar{D}$ candidate), the reconstructed $M_{\rm bc}(\bar{D})$ and $M_{\rm bc}(D)$ will lie on the diagonal. There are horizontal

and vertical bands centered at $M_{\rm bc}(\bar{D}) = M_{D^0}$ and $M_{\rm bc}(D) = M_{D^0}$, respectively. These bands contain DT candidates in which the $\bar{D}$ (D) candidate was reconstructed correctly, but the D ($\bar{D}$) was not. Fig. 5 [16] illustrates the $M_{\rm bc}$ distribution for all DT $D^0\bar{D}^0$ candidates combined and for all DT D^+D^- candidates combined. The figure emphasizes the fact that the DT backgrounds are indeed very small.

6.2.3. *Absolute branching fractions*

A detailed study of systematic uncertainties, including the final state radiation effects, has been performed for this measurement [16]. The signal yields for single and double tags and the efficiencies determined from Monte Carlo simulations are combined in a χ^2 fit [43]. This fit includes both statistical and systematic uncertainties. The fit extracts the branching fractions for the three D^0 and six D^+ decay modes studied in this analysis and the produced number of $D^0\bar{D}^0$ and D^+D^- pairs. The results of the fit to data are shown in Table 1 [16]. The χ^2 of the fit, including systematic uncertainties, is 39.2 for 52 degrees of freedom, corresponding to a confidence level of 98%. The results of the reference branching fractions from CLEO-c are,

$$\mathcal{B}(D^0 \to K^-\pi^+) = (3.891 \pm 0.035 \pm 0.059 \pm 0.035)\%,$$
$$\mathcal{B}(D^+ \to K^-\pi^+\pi^+) = (9.14 \pm 0.10 \pm 0.16 \pm 0.07)\%,$$

where the errors are statistical, systematic, and from final state radiation respectively [16]. These results agree well with (and supersede) previous CLEO-c measurements based on a 56 pb^{-1} sub-sample [41]. The measurement of the reference branching fraction $\mathcal{B}(D^0 \to K^-\pi^+)$ is smaller than, but consistent with, that reported by the BABAR Collaboration [44], $\mathcal{B}(D^0 \to K^-\pi^+) = (4.007 \pm 0.037 \pm 0.072)\%$.

6.2.4. *CP asymmetries*

Although this analysis assumes equal rates for decays to charge-conjugate final states f and $\overline{f}$, the separately determined yields and efficiencies for charge-conjugate decays allow the calculation of CP asymmetries,

$$A_{CP}(f) \equiv \frac{n(f) - n(\overline{f})}{n(f) + n(\overline{f})}, \tag{7}$$

for each mode f. In this expression, the CP asymmetry $A_{CP}(f)$ is calculated from $n(f)$ and $n(\overline{f})$, the single tag yields obtained for the charge-conjugate modes f and $\overline{f}$, after subtraction of backgrounds and correction for efficiencies.

Most systematic uncertainties cancel between f and $\overline{f}$, with the exception of charged pion and kaon tracking and particle identification. The CP asymmetries obtained in this analysis are given in the last column of Table 1. The uncertainties are of order 1% in all modes, and no mode shows evidence of CP violation. CLEO-c is insensitive to asymmetries at the level expected from the standard model, the largest of which are a few tenths of a percent in modes with a K^0_S [45].

Table 1. Fitted branching fractions and $D\bar{D}$ pair yields. For $N_{D^0\bar{D}^0}$ and $N_{D^+D^-}$, uncertainties are statistical and systematic, respectively. For branching fractions and ratios, the systematic uncertainties are divided into the contribution from FSR (third uncertainty) and all others combined (second uncertainty). The column of fractional systematic errors combines all systematic errors, including FSR. The next to last column, $\Delta_{\rm FSR}$, is the relative shift in the fit results when FSR is not included in the Monte Carlo simulations used to determine efficiencies. The last column is the CP asymmetries obtained in this analysis. (Table from reference, see text.)

Parameter	Fitted Value	Fractional Error Stat.(%)	Fractional Error Syst.(%)	$\Delta_{\rm FSR}$ (%)	A_{CP} (%)
$N_{D^0\bar{D}^0}$	$(1.031 \pm 0.008 \pm 0.013) \times 10^6$	0.8	1.3	+0.1	
$\mathcal{B}(D^0 \to K^-\pi^+)$	$(3.891 \pm 0.035 \pm 0.059 \pm 0.035)\%$	0.9	1.8	−3.0	$-0.4 \pm 0.5 \pm 0.9$
$\mathcal{B}(D^0 \to K^-\pi^+\pi^0)$	$(14.57 \pm 0.12 \pm 0.38 \pm 0.05)\%$	0.8	2.7	−1.1	$0.2 \pm 0.4 \pm 0.8$
$\mathcal{B}(D^0 \to K^-\pi^+\pi^+\pi^-)$	$(8.30 \pm 0.07 \pm 0.19 \pm 0.07)\%$	0.9	2.4	−2.4	$0.7 \pm 0.5 \pm 0.9$
$N_{D^+D^-}$	$(0.819 \pm 0.008 \pm 0.010) \times 10^6$	1.0	1.2	+0.1	
$\mathcal{B}(D^+ \to K^-\pi^+\pi^+)$	$(9.14 \pm 0.10 \pm 0.16 \pm 0.07)\%$	1.1	1.9	−2.3	$-0.5 \pm 0.4 \pm 0.9$
$\mathcal{B}(D^+ \to K^-\pi^+\pi^+\pi^0)$	$(5.98 \pm 0.08 \pm 0.16 \pm 0.02)\%$	1.3	2.8	−1.0	$1.0 \pm 0.9 \pm 0.9$
$\mathcal{B}(D^+ \to K^0_S\pi^+)$	$(1.526 \pm 0.022 \pm 0.037 \pm 0.009)\%$	1.4	2.5	−1.8	$-0.6 \pm 1.0 \pm 0.3$
$\mathcal{B}(D^+ \to K^0_S\pi^+\pi^0)$	$(6.99 \pm 0.09 \pm 0.25 \pm 0.01)\%$	1.3	3.5	−0.4	$0.3 \pm 0.9 \pm 0.3$
$\mathcal{B}(D^+ \to K^0_S\pi^+\pi^+\pi^-)$	$(3.122 \pm 0.046 \pm 0.094 \pm 0.019)\%$	1.5	3.0	−1.9	$0.1 \pm 1.1 \pm 0.6$
$\mathcal{B}(D^+ \to K^+K^-\pi^+)$	$(0.935 \pm 0.017 \pm 0.024 \pm 0.003)\%$	1.8	2.6	−1.2	$-0.1 \pm 1.5 \pm 0.8$
$\mathcal{B}(D^0 \to K^-\pi^+\pi^0)/\mathcal{B}(K^-\pi^+)$	$3.744 \pm 0.022 \pm 0.093 \pm 0.021$	0.6	2.6	+1.9	
$\mathcal{B}(D^0 \to K^-\pi^+\pi^+\pi^-)/\mathcal{B}(K^-\pi^+)$	$2.133 \pm 0.013 \pm 0.037 \pm 0.002$	0.6	1.7	+0.5	
$\mathcal{B}(D^+ \to K^-\pi^+\pi^+\pi^0)/\mathcal{B}(K^-\pi^+\pi^+)$	$0.654 \pm 0.006 \pm 0.018 \pm 0.003$	0.9	2.7	+1.4	
$\mathcal{B}(D^+ \to K^0_S\pi^+)/\mathcal{B}(K^-\pi^+\pi^+)$	$0.1668 \pm 0.0018 \pm 0.0038 \pm 0.0003$	1.1	2.3	+0.5	
$\mathcal{B}(D^+ \to K^0_S\pi^+\pi^0)/\mathcal{B}(K^-\pi^+\pi^+)$	$0.764 \pm 0.007 \pm 0.027 \pm 0.005$	0.9	3.5	+2.0	
$\mathcal{B}(D^+ \to K^0_S\pi^+\pi^+\pi^-)/\mathcal{B}(K^-\pi^+\pi^+)$	$0.3414 \pm 0.0039 \pm 0.0093 \pm 0.0004$	1.1	2.7	+0.4	
$\mathcal{B}(D^+ \to K^+K^-\pi^+)/\mathcal{B}(K^-\pi^+\pi^+)$	$0.1022 \pm 0.0015 \pm 0.0022 \pm 0.0004$	1.5	2.2	+1.1	

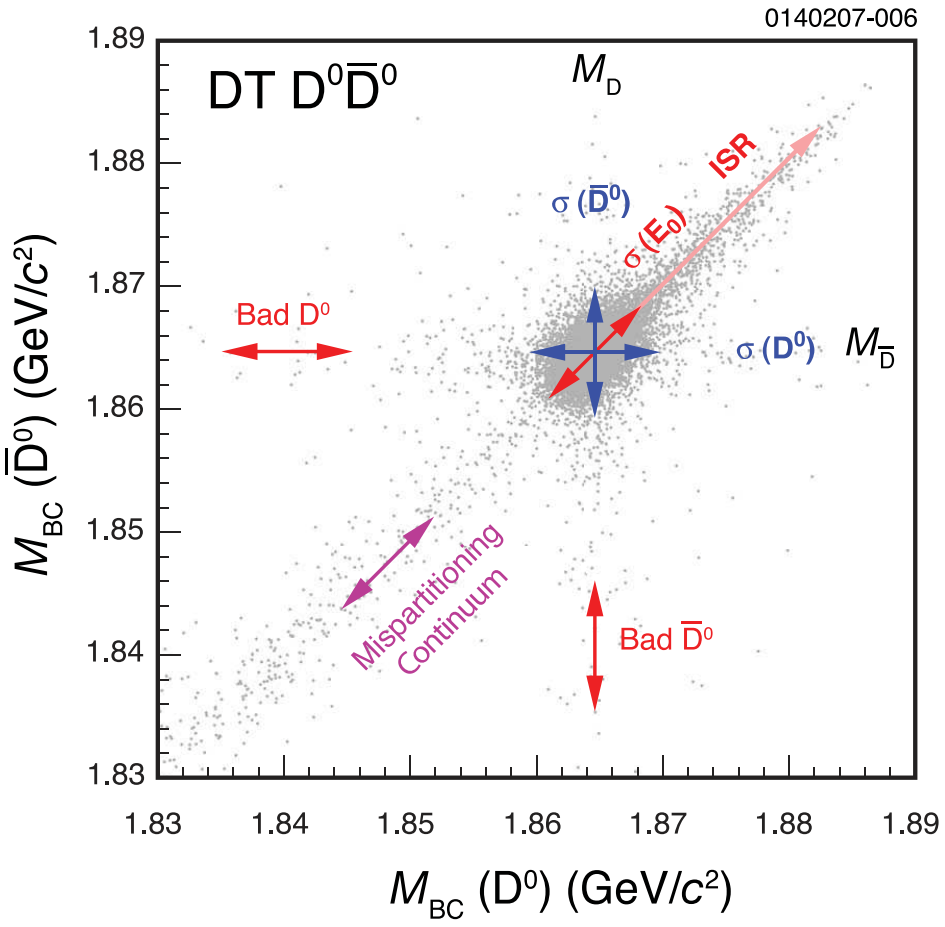

Fig. 4. Scatter plot of $M_{\rm bc}(\bar{D})$ vs. $M_{\rm bc}(D)$ for $D^0\bar{D}^0$ double tag candidates. Signal candidates are concentrated at $M_{\rm bc}(\bar{D}) = M_{\rm bc}(D) = M_D$. Beam energy smearing ($\sigma(E_0)$) smears candidates along the $M_{\rm bc}(\bar{D})$ vs. $M_{\rm bc}(D)$ diagonal. Initial state radiation (ISR) spreads candidates further along the diagonal above the concentration of signal candidates. Detector resolution smears an candidate parallel to the $M_{\rm bc}(\bar{D})$ axis ($\sigma(\bar{D}^0)$) and parallel to the $M_{\rm bc}(D)$ axis ($\sigma(D^0)$). Since the D^0 and $\bar{D}^0$ resolutions are equal, the resulting distribution is isotropic. Candidates with either the D^0 or $\bar{D}^0$ properly reconstructed and the other improperly reconstructed are spread along the lines $M_{\rm bc}(\bar{D}) = M_D$ or $M_{\rm bc}(D) = M_D$. Candidates that are mispartitioned (*i.e.*, where some particles are interchanged between the D^0 and the $\bar{D}^0$) are spread along the diagonal. Finally, some of the candidates smeared along the diagonal are from continuum events (*i.e.*, annihilations to $u\bar{u}$, $d\bar{d}$, and $s\bar{s}$ quark pairs) where all particles in the final state are found and used. (Figure from reference, see text.)

6.2.5. *Cross section for $D\bar{D}$ production*

CLEO-c also obtains the $e^+e^- \to D\bar{D}$ cross sections by dividing the fitted values of $N_{D^0\bar{D}^0}$ and $N_{D^+D^-}$ by the collected luminosity, $\int \mathcal{L}dt = 281.5 \pm 2.8$ pb^{-1} [16]. Thus,

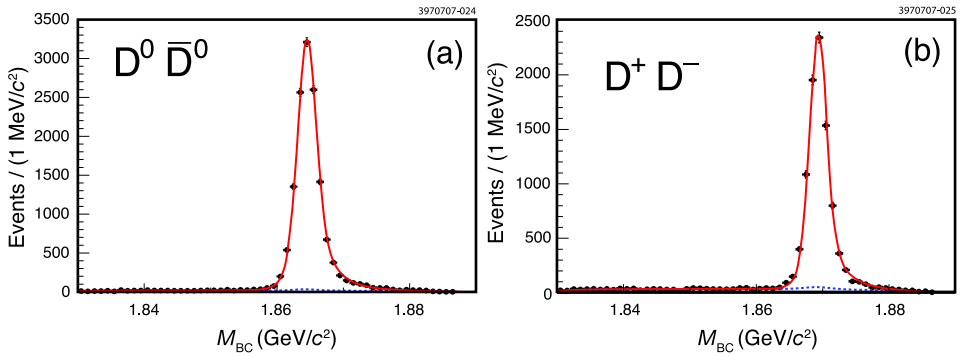

Fig. 5. Projections of double tag candidate masses on the $M_{\rm bc}(D)$ axis for (a) all double tag $D^0\bar{D}^0$ modes and (b) all double tag D^+D^- modes. In each plot, the lines are projections of the fit results, the dashed line is the background contribution, and the solid line is the sum of signal and background. (Figure from reference, see text.)

at $E_{\rm cm} = 3774 \pm 1$ MeV, the values of the production cross sections are given in Table 2, which are in good agreement with BES [46] measurements. (The uncertainty of 1 MeV corresponds to the range of center-of-mass energies in the data sample.)

Table 2. Production cross sections for $e^+e^- \to D\bar{D}$ and the ratio of D^+D^- to $D^0\bar{D}^0$ cross sections. The uncertainties are statistical and systematic, respectively. The charged and neutral cross sections have a correlation coefficient of 0.57 stemming from systematic uncertainties and from the common use of the luminosity measurement. (Table from reference, see text.)

Quantity	Value
$\sigma(e^+e^- \to D^0\bar{D}^0)$	$(3.66 \pm 0.03 \pm 0.06)$ nb
$\sigma(e^+e^- \to D^+\bar{D}^-)$	$(2.91 \pm 0.03 \pm 0.05)$ nb
$\sigma(e^+e^- \to D\bar{D})$	$(6.57 \pm 0.04 \pm 0.10)$ nb
$\sigma(e^+e^- \to D^+\bar{D}^-)/\sigma(e^+e^- \to D^0\bar{D}^0)$	$0.79 \pm 0.01 \pm 0.01$

6.2.6. *Non-$D\bar{D}$ decays of* $\psi(3700)$

CLEO-c has reported a measurement of the cross section, $\sigma(e^+e^- \to \psi(3770) \to$ hadrons) $\equiv \sigma_{3770} = (6.38 \pm 0.08^{+0.41}_{-0.30})$ nb in Ref. 47. Then, using the results in this analysis [16], which gave $\sigma(e^+e^- \to \psi(3770) \to D\bar{D}) \equiv \sigma_{D\bar{D}} = (6.57 \pm 0.04 \pm 0.10)$ nb, CLEO-c could obtain the cross section for non-$D\bar{D}$ decays of $\psi(3770)$, $\sigma_{\text{non-}D\bar{D}} \equiv \sigma_{3770} - \sigma_{D\bar{D}}$. Recently CLEO-c has updated the measurement of non-$D\bar{D}$ decays of $\psi(3770)$ [47,48]. Because of different efficiencies for $D\bar{D}$ and non-$D\bar{D}$ final states, the value for σ_{3770} in Ref. 47 changes slightly, to $\sigma_{3770} = (6.36 \pm 0.08^{+0.41}_{-0.30})$ nb. Consequently, the value of $\Gamma_{ee}(\psi(3770))$ changes slightly to $(0.203 \pm 0.003^{+0.041}_{-0.027})$ keV. The new value for $\sigma_{\text{non-}D\bar{D}}$ is $(-0.21 \pm 0.09^{+0.41}_{-0.30})$ nb. Dividing this difference by σ_{3770} yields the branching fraction $\mathcal{B}(\psi(3770) \to \text{non-}D\bar{D}) =$

$(-3.3 \pm 1.4^{+6.6}_{-4.8})\%$ which corresponds to $\mathcal{B}(\psi(3770) \to \text{non-}D\bar{D}) < 9\%$ at 90% confidence level when considering only physical (positive) values [47,48].

6.3. *Absolute D_s^+ hadronic branching fractions*

Using the double tag technique similar to what was done for the D^0 and D^+ hadronic branching fractions [16], CLEO-c has determined the absolute hadronic branching fractions for D_s^+ meson decays [49]. This CLEO-c analysis used a sample of (298 ± 3) pb^{-1} of e^+e^- collision data taken at a center-of-mass energy of 4170 MeV. At this energy the dominant D_s production mechanism is the process $e^+e^- \to D_s^{*\pm}D_s^{\mp}$ with a cross section of about 1 nb [20]; the D_s^* then decays to either γD_s or $\pi^0 D_s$ in a $\sim 16:1$ ratio [23]. The transition π^0 or photon was not reconstructed. The eight hadronic decays considered in this analysis by CLEO-c are $D_s^+ \to K_S^0K^+$, $D_s^+ \to K_S^0K^-\pi^+\pi^+$, $D_s^+ \to K^+K^-\pi^+$, $D_s^+ \to K^+\pi^-\pi^+$, $D_s^+ \to K^+K^-\pi^+\pi^0$, $D_s^+ \to \pi^+\pi^-\pi^+$, $D_s^+ \to \eta\pi^+$, and $D_s^+ \to \eta'\pi^+$. Except where noted, mention of a decay implies the charge-conjugate process as well. A total of 16 single tag modes and 64 double tag modes were used.

6.3.1. *Single tag yields*

The single tag (ST) signal yields are extracted from the D_s invariant mass distributions. For ST yield extraction, at most one single tag candidate per mode and charge is allowed per event. If there are multiple candidates, the one with $M_{\text{recoil}}(D_s)$ closest to $M_{D_s^*}$ is chosen. An unbinned maximum likelihood fit is then performed on the invariant mass spectrum of the candidates in each mode. The signal shape is determined from Monte Carlo simulations, but the D_s mass is allowed to float in the fit. The background is modeled with a linear function in all modes except $K^+K^-\pi^+\pi^0$ and $\pi^+\pi^0\pi^0$ where a quadratic form is used instead. The same background shape is used for both charges in a given mode. The reconstructed candidate masses $M(D_s)$ and ST yield fits are shown in Fig. 6 [49]. Efficiencies for ST modes range from 5.3% to 51%.

6.3.2. *Double tag yields*

Double tag yields are extracted through a cut-and-count procedure by defining a signal region in the two-dimensional plane of the two D_s candidate masses, $M(D_s^+)$ vs. $M(D_s^-)$. At most one double tag candidate is allowed per event. Amongst multiple candidates, the combination with average mass $\hat{M} = (M(D_s^+) + M(D_s^-))/2$ closest to M_{D_s} is chosen. The distribution of $M(D_s^-)$ versus $M(D_s^+)$ for all DT candidates, along with the signal and sideband regions, is shown in Fig. 7 [49]. The combinatoric background has structure in $\hat{M}$, but is flat in the mass difference $\Delta M = M(D_s^+) - M(D_s^-)$; in particular simulations verify that the multiple candidate selection does not cause backgrounds to peak in ΔM. Both signal and sideband regions require $|\hat{M} - M_{D_s}| < 12$ MeV/c^2. The signal region is $|\Delta M| < 30$ MeV/c^2,

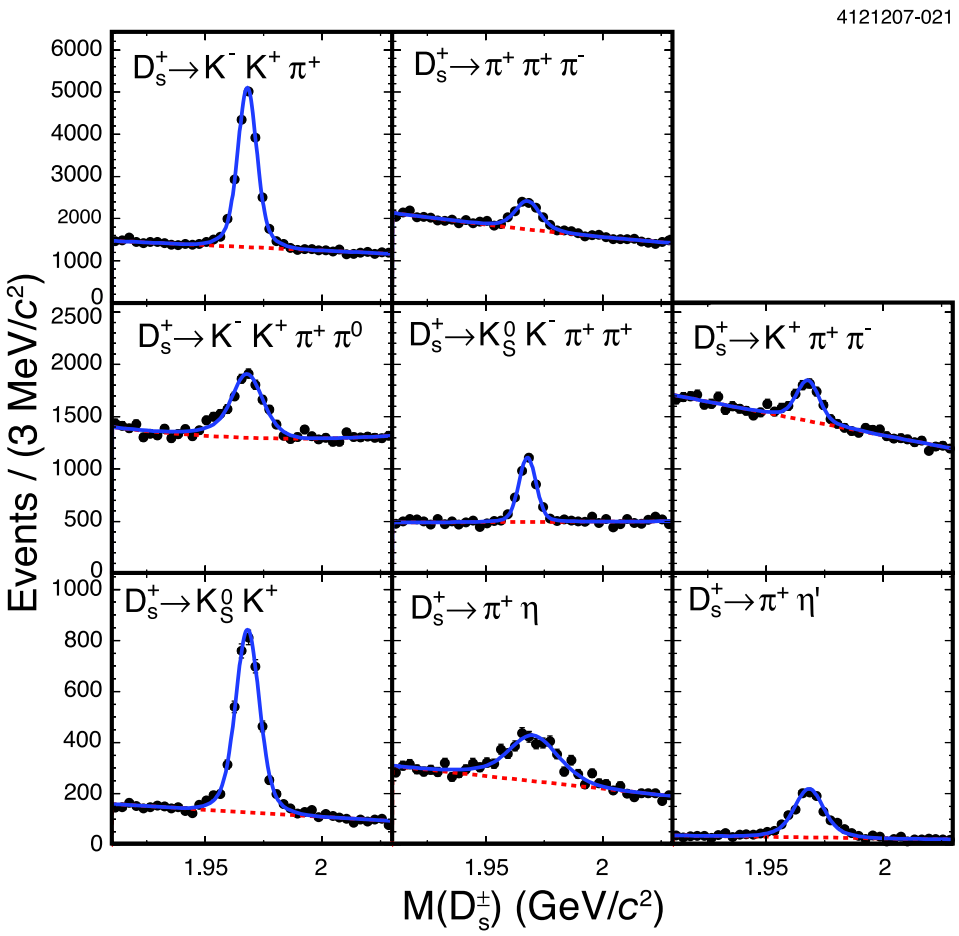

Fig. 6. Invariant masses of the $D_s^\pm$ candidates in data in ST modes. Charge-conjugate modes are combined. The fits for yields are shown as the dashed red lines (background component) and solid blue lines (signal plus background). The total ST yield is $(30.9 \pm 0.3) \times 10^3$ events. (Figure from reference, see text.)

while the sideband region is $50 < |\Delta M| < 140\text{MeV}/c^2$. Efficiencies for DT modes range from 0.3% to 38%.

6.3.3. *Absolute D_s^+ hadronic branching fractions*

All yields and efficiencies are combined in a likelihood fit to extract the D_s branching fractions. The branching fraction results from this fit is presented in Table 3 [49]. Instead of giving a $D_s^+ \to \phi\pi^+$ branching fractions as a reference modes, CLEO-c provides partial branching fractions $\mathcal{B}_{\Delta M}$, which are defined as the branching fraction for $K^-K^+\pi^+$ events where the K^+K^- pair satisfies

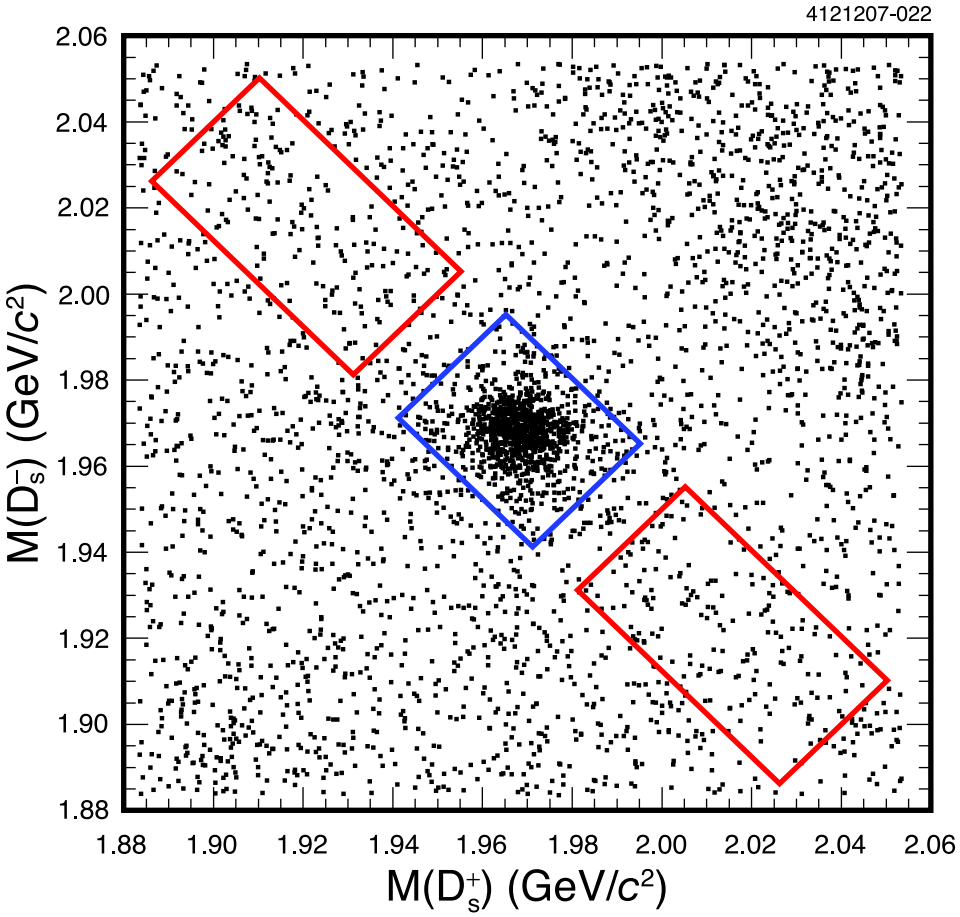

Fig. 7. Masses of the $M(D_s^-)$ and $M(D_s^+)$ candidates for all 64 DT modes in data. The rectangles show the signal region (center) and two sideband regions (diagonally offset). There are 1089 events in the signal region and 339 events in the combined sideband regions. (Figure from reference, see text.)

$|M(K^+K^-) - 1019.5\ \mathrm{MeV}/c^2| < \Delta M\ (\mathrm{MeV}/c^2)$; the values obtained are listed in Table 4 [49].

6.3.4. *CP asymmetries and cross section for $D_s^* D_s$ production*

The separated yields and efficiencies for D_s^+ and D_s^- allow CLEO-c to compute direct CP asymmetries in D_s decays which are shown in the last column of Table 4 [49]. No significant CP asymmetries are observed. In addition to the branching fractions, CLEO-c obtains the number of $D_s^* D_s$ events $N_{D_s^* D_s} = (2.93 \pm 0.14 \pm 0.06) \times 10^5$. Combined with the luminosity, $\mathcal{L}_{\mathrm{int}} = (298 \pm 3)\ \mathrm{pb}^{-1}$, CLEO-c obtains the cross-section $\sigma_{D_s^* D_s}(E_{\mathrm{cm}} = 4.17\ \mathrm{GeV}) = (0.983 \pm 0.046 \pm 0.021 \pm 0.010)$ nb; in order, the

Table 3. Branching fractions for D_s decays and charge asymmetries $\mathcal{A}_{CP}$ from CLEO-c. Uncertainties are statistical and systematic, respectively. (Table from reference, see text.)

Mode	This result $\mathcal{B}$ (%)	$\mathcal{B}/\mathcal{B}(K^+K^-\pi^+)$	$\mathcal{A}_{CP}$ (%)
$\mathcal{B}(D_s^+ \to K_S^0 K^+)$	$1.49 \pm 0.07 \pm 0.05$	$0.270 \pm 0.009 \pm 0.008$	$+4.9 \pm 2.1 \pm 0.9$
$\mathcal{B}(D_s^+ \to K^+K^-\pi^+)$	$5.50 \pm 0.23 \pm 0.16$	1	$+0.3 \pm 1.1 \pm 0.8$
$\mathcal{B}(D_s^+ \to K^+K^-\pi^+\pi^0)$	$5.65 \pm 0.29 \pm 0.40$	$1.03 \pm 0.05 \pm 0.08$	$-5.9 \pm 4.2 \pm 1.2$
$\mathcal{B}(D_s^+ \to K_S^0 K^-\pi^+\pi^+)$	$1.64 \pm 0.10 \pm 0.07$	$0.298 \pm 0.014 \pm 0.011$	$-0.7 \pm 3.6 \pm 1.1$
$\mathcal{B}(D_s^+ \to \pi^+\pi^-\pi^+)$	$1.11 \pm 0.07 \pm 0.04$	$0.202 \pm 0.011 \pm 0.009$	$+2.0 \pm 4.6 \pm 0.7$
$\mathcal{B}(D_s^+ \to \pi^+\eta)$	$1.58 \pm 0.11 \pm 0.18$	$0.288 \pm 0.018 \pm 0.033$	$-8.2 \pm 5.2 \pm 0.8$
$\mathcal{B}(D_s^+ \to \pi^+\eta')$	$3.77 \pm 0.25 \pm 0.30$	$0.69 \pm 0.04 \pm 0.06$	$-5.5 \pm 3.7 \pm 1.2$
$\mathcal{B}(D_s^+ \to K^+\pi^+\pi^-)$	$0.69 \pm 0.05 \pm 0.03$	$0.125 \pm 0.009 \pm 0.005$	$+11.2 \pm 7.0 \pm 0.9$

Table 4. Partial branching fractions $\mathcal{B}_{\Delta M}$ for $K^-K^+\pi^+$ events with K^+K^- mass within ΔM MeV/c^2 of the ϕ mass. Uncertainties are statistical and systematic, respectively. (Table from reference, see text.)

Value	This Result $\mathcal{B}$ (%)
$\mathcal{B}_5$	$1.69 \pm 0.08 \pm 0.06$
$\mathcal{B}_{10}$	$1.99 \pm 0.10 \pm 0.05$
$\mathcal{B}_{15}$	$2.14 \pm 0.10 \pm 0.05$
$\mathcal{B}_{20}$	$2.24 \pm 0.11 \pm 0.06$

uncertainties are statistical, systematic due to this measurement, and systematic due to the luminosity measurement [16]. The cross section is consistent with earlier CLEO-c results obtained via a scan of this energy region [20].

7. Cabibbo Suppressed D^0, D^+ and D_s^+ Decays

Hadronic singly Cabibbo suppressed decays of charmed mesons hold the potential for future observation of direct CP violation in the D system which is not associated with $D^0\bar{D}^0$ mixing [45,50,51,52]. It also offers new ground for studying strong dynamics in hadronic decays, in particular, the issue of flavor $SU(3)$ symmetry breaking in D decays [36,37,53,54,55,56].

7.1. D^0 and D^+ decays to pions

Using the 281 pb^{-1} $\psi(3770)$ data sample, CLEO-c measured "singly Cabibbo suppressed" (SCS) decays of D^0 and D^+ to multipion final states [57]. The $M_{\rm bc}$ distributions are shown in Fig. 8 [57]. Further more, CLEO-c searched the $D^+ \to \pi^+\pi^+\pi^-\pi^0$, $D^0 \to \pi^+\pi^-\pi^0\pi^0$, and $D^0 \to \pi^+\pi^+\pi^-\pi^-\pi^0$ modes for η and ω decays. The yields are extracted by selecting events that are within 2.5 times the Gaussian width of the D mass and taking the difference in yields between the number of such events in the ΔE signal and ΔE sideband regions. The sideband distributions are normalized to account for the different range of ΔE between signal and sidebands regions.

Relative branching fractions are computed and listed in Table 5 [57]. To compute

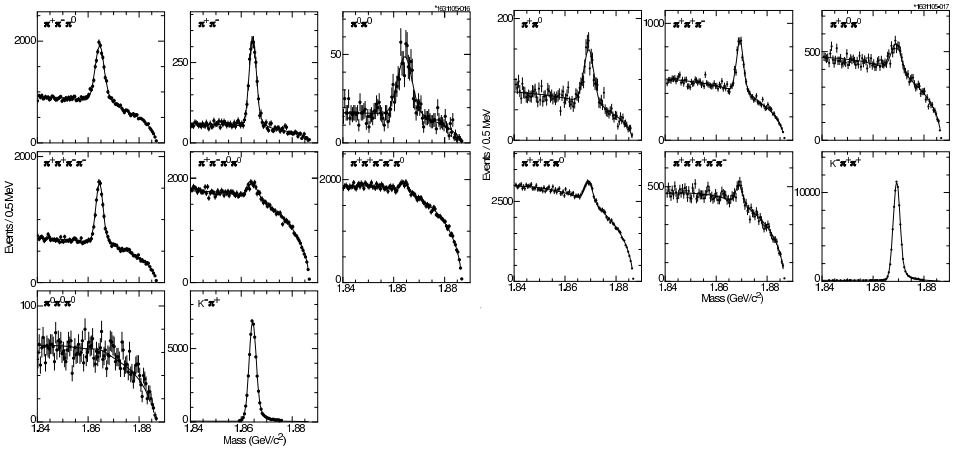

Fig. 8. $M_{\rm bc}$ distributions for D^0 (plots on the left) and D^+ (plots on the right) modes from data. The points are the data and the superimposed lines are the fits. (Figure from reference, see text.)

the absolute branching fractions, CLEO-c used $\mathcal{B}(D^0 \to K^-\pi^+) = (3.84 \pm 0.07)\%$ and $\mathcal{B}(D^+ \to K^-\pi^+\pi^+) = (9.4 \pm 0.3)\%$, which were obtained using weighted averages of the PDG 2004 values [58] and the CLEO measurements [41]. For unobserved modes, CLEO-c set 90% confidence level upper limits.

Table 5. Measured relative and absolute branching fractions for neutral and charged D modes. Uncertainties are statistical, experimental systematic, normalization mode uncertainty, and uncertainty from CP correlations (for D^0 modes only). For the relative branching fractions, the normalization mode uncertainty is omitted. (Table from reference, see text.)

Mode	$\mathcal{B}_{\rm mode}/\mathcal{B}_{\rm ref}$ (%)	$\mathcal{B}_{\rm mode}$ (10^{-3})
$D^0 \to \pi^+\pi^-$	$3.62 \pm 0.10 \pm 0.07 \pm 0.04$	$1.39 \pm 0.04 \pm 0.04 \pm 0.03 \pm 0.01$
$D^0 \to \pi^0\pi^0$	$2.05 \pm 0.13 \pm 0.16 \pm 0.02$	$0.79 \pm 0.05 \pm 0.06 \pm 0.01 \pm 0.01$
$D^0 \to \pi^+\pi^-\pi^0$	$34.4 \pm 0.5 \pm 1.2 \pm 0.3$	$13.2 \pm 0.2 \pm 0.5 \pm 0.2 \pm 0.1$
$D^0 \to \pi^+\pi^+\pi^-\pi^-$	$19.1 \pm 0.4 \pm 0.6 \pm 0.2$	$7.3 \pm 0.1 \pm 0.3 \pm 0.1 \pm 0.1$
$D^0 \to \pi^+\pi^-\pi^0\pi^0$	$25.8 \pm 1.5 \pm 1.8 \pm 0.3$	$9.9 \pm 0.6 \pm 0.7 \pm 0.2 \pm 0.1$
$D^0 \to \pi^+\pi^+\pi^-\pi^-\pi^0$	$10.7 \pm 1.2 \pm 0.5 \pm 0.1$	$4.1 \pm 0.5 \pm 0.2 \pm 0.1 \pm 0.0$
$D^0 \to \omega\pi^+\pi^-$	$4.1 \pm 1.2 \pm 0.4 \pm 0.0$	$1.7 \pm 0.5 \pm 0.2 \pm 0.0 \pm 0.0$
$D^0 \to \eta\pi^0$	$1.47 \pm 0.34 \pm 0.11 \pm 0.01$	$0.62 \pm 0.14 \pm 0.05 \pm 0.01 \pm 0.01$
$D^0 \to \pi^0\pi^0\pi^0$	-	< 0.35 (90% CL)
$D^0 \to \omega\pi^0$	-	< 0.26 (90% CL)
$D^0 \to \eta\pi^+\pi^-$	-	< 1.9 (90% CL)
$D^+ \to \pi^+\pi^0$	1.33±0.07±0.06	1.25±0.06±0.07±0.04
$D^+ \to \pi^+\pi^+\pi^-$	3.52±0.11±0.12	3.35±0.10±0.16±0.12
$D^+ \to \pi^+\pi^0\pi^0$	5.0±0.3±0.3	4.8±0.3±0.3±0.2
$D^+ \to \pi^+\pi^+\pi^-\pi^0$	12.4±0.5±0.6	11.6±0.4±0.6±0.4
$D^+ \to \pi^+\pi^+\pi^+\pi^-\pi^-$	1.73±0.20±0.17	1.60±0.18±0.16±0.06
$D^+ \to \eta\pi^+$	3.81±0.26±0.21	3.61±0.25±0.23±0.12
$D^+ \to \omega\pi^+$	-	< 0.34 (90% CL)

7.2. D^0 and D^+ decays to final states containing η and η' mesons

Using 281 pb^{-1} of data collected at the $\psi(3770)$ resonance, CLEO-c has done the complete study of D^0 and D^+ meson decays to final states containing η and η' mesons [59]. In this analysis, the signal yields are extracted by fitting the $M_{\rm bc}$ distributions after selecting events consistent with $\Delta E = 0$. The observed signals are shown in Figs. 9 [59] and the branching fractions are summarized in Tab. 6 [59].

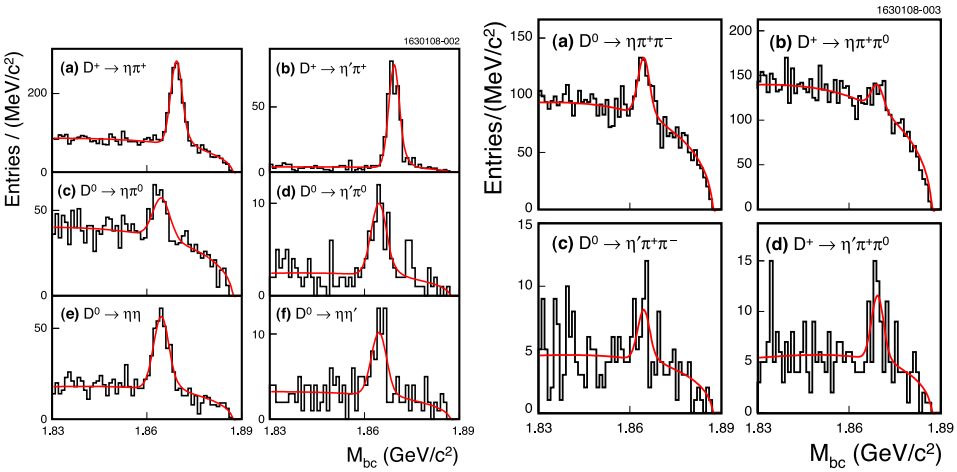

Fig. 9. Distributions of $M_{\rm bc}$ for the two-body Cabibbo suppressed decay modes (plots on left): (a) $D^+ \to \eta\pi^+$, (b) $D^+ \to \eta'\pi^+$, (c) $D^0 \to \eta\pi^0$, (d) $D^0 \to \eta'\pi^0$, (e) $D^0 \to \eta\eta$, and (f) $D^0 \to \eta\eta'$; and for the three-body Cabibbo suppressed decay modes (plots on right): (a) $D^0 \to \eta\pi^+\pi^-$, (b) $D^+ \to \eta\pi^+\pi^0$, (c) $D^0 \to \eta'\pi^+\pi^-$, and (d) $D^+ \to \eta'\pi^+\pi^0$. (Figure from reference, see text.)

7.3. D^0 and D^+ decays to two kaons

CLEO-c has studied Cabibbo suppressed two-body decays of D^0 and D^+ mesons to a pair of kaons by using 281 pb^{-1} of data collected at the $\psi(3770)$ resonance [60]. In particular, the decays $D^0 \to K^-K^+$, $D^0 \to K^0_S K^0_S$, and $D^+ \to K^+K^0_S$ have been analyzed. In addition to being Cabibbo suppressed, the $D^0 \to K^0_S K^0_S$ mode is strongly suppressed due to destructive interference in the $SU(3)$ limit between the two dominating exchange amplitudes for this decay. Figure 10 [60] shows the $M_{\rm bc}$ distributions for these three modes. The measured branching fractions are [60]:

$$\mathcal{B}(D^0 \to K^+K^-) = (4.08 \pm 0.08 \pm 0.09) \times 10^{-3},$$
$$\mathcal{B}(D^0 \to K^0_S K^0_S) = (1.46 \pm 0.32 \pm 0.09) \times 10^{-4},$$
$$\mathcal{B}(D^+ \to K^+K^0_S) = (3.14 \pm 0.09 \pm 0.08) \times 10^{-3}.$$

Table 6. Summary of yields and branching fraction measurements of D^0 and D^+ meson decays to final states with η and η'. For $D^0 \to \eta\eta$ and $D^0 \to \eta\eta'$, also show the individual results obtained from the two η submodes. The first uncertainty is statistical and the second is systematic. (Table from reference, see text.)

Mode	Yield	Branching Fraction (10^{-4})
$D^+ \to \eta\pi^+$	1033 ± 42	$34.3 \pm 1.4 \pm 1.7$
$D^+ \to \eta'\pi^+$	352 ± 20	$44.2 \pm 2.5 \pm 2.9$
$D^0 \to \eta\pi^0$	156 ± 24	$6.4 \pm 1.0 \pm 0.4$
$D^0 \to \eta'\pi^0$	50 ± 9	$8.1 \pm 1.5 \pm 0.6$
$D^0 \to \eta\eta$	255 ± 22	$16.7 \pm 1.4 \pm 1.3$
$(\gamma\gamma)(\gamma\gamma)$	141 ± 17	15.3 ± 1.8(stat.)
$(\gamma\gamma)(\pi^+\pi^-\pi^0)$	115 ± 13	19.0 ± 2.2(stat.)
$D^0 \to \eta\eta'$	46 ± 9	$12.6 \pm 2.5 \pm 1.1$
$(\gamma\gamma)(\gamma\gamma)$	33 ± 8	14.8 ± 3.3(stat.)
$(\gamma\gamma)(\pi^+\pi^-\pi^0)$	14 ± 5	10.5 ± 3.5(stat.)
$D^0 \to \eta\pi^+\pi^-$	257 ± 32	$10.9 \pm 1.3 \pm 0.9$
$D^+ \to \eta\pi^+\pi^0$	149 ± 34	$13.8 \pm 3.1 \pm 1.6$
$D^0 \to \eta'\pi^+\pi^-$	21 ± 8	$4.5 \pm 1.6 \pm 0.5$
$D^+ \to \eta'\pi^+\pi^0$	33 ± 9	$15.7 \pm 4.3 \pm 2.5$

7.4. *Suppressed decays of D_s^+ mesons to two pseudoscalar mesons*

Using 298 pb^{-1} of data produced near the center-of-mass energy $E_{\rm cm} = 4170$ MeV, CLEO-c has performed a study of D_s^+ meson decays to a pair of pseudoscalar mesons, made the first observations of the singly Cabibbo suppressed, color-favored decays $D_s^+ \to K^+\eta$, $D_s^+ \to K^+\eta'$, and $D_s^+ \to \pi^+ K_S^0$, and observed strong evidence (4.7 standard deviations (σ)) for the singly Cabibbo suppressed, color-mixed decay $D_s^+ \to K^+\pi^0$ [28]. In this analysis, CLEO-c measured the ratio of the branching fraction of each singly Cabibbo suppressed decay to that of the corresponding favored decay, expected to be, and found to be, of order $|V_{cd}/V_{cs}|^2 \approx 1/20$. The decay $D_s^+ \to \pi^+\pi^0$ requires a change in isospin of 2 units, and is thus "isospin-forbidden", and expected to be substantially suppressed. The search for this decay revealed no firm evidence for it, and set an upper limit for this decay mode.

The resulting $M(D_s)$ distributions for the Cabibbo favored and Cabibbo suppressed D_s modes are shown in Figs. 11 [28]. A binned maximum likelihood fit (2 MeV/c^2 bins) has been performed to extract signal yields from the $M(D_s)$ distributions. For the signal, CLEO-c used the sum of two Gaussians for the line shape. The signal shape parameters are determined by fits to $M(D_s)$ distributions obtained from Monte Carlo simulation, with the proviso that the peak location of the primary Gaussian is allowed to shift in the fits to the Cabibbo favored modes, and all other peak locations are shifted by the same amount. For the background, CLEO-c used a second-degree polynomial function, allowing the overall scale, and the coefficient of the linear term relative to the constant term, to float in the fits to the data. All fits have a χ^2/d.o.f. ≈ 1.0.

For the modes with η or $\eta'(\eta' \to \pi^+\pi^-\eta)$ in the final state, the η candidates are

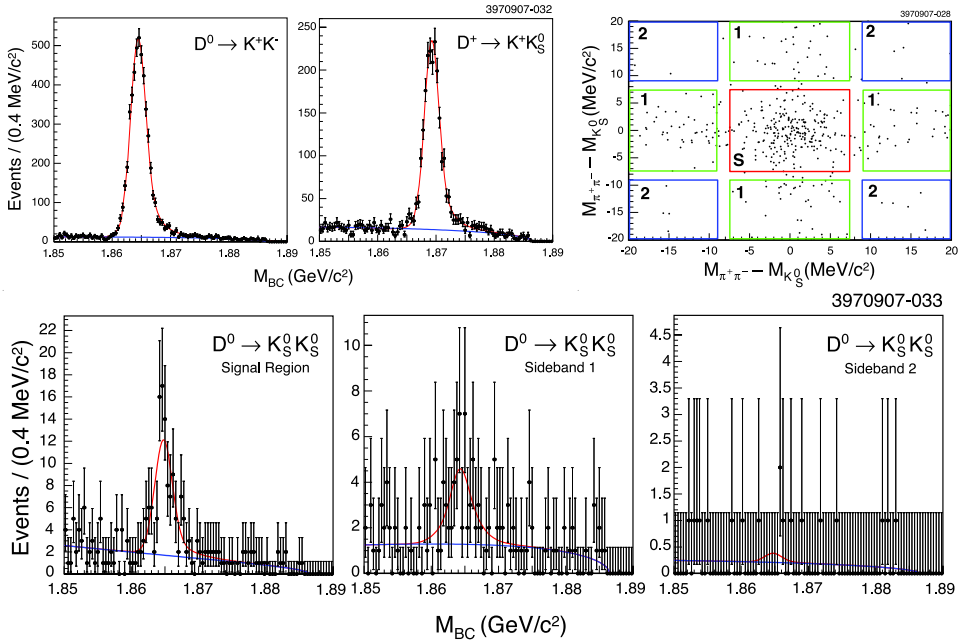

Fig. 10. $M_{\rm bc}$ plots for data (upper plots), left to right: $D^0 \to K^+K^-$ and $D^+ \to K^+K^0_S$. $D^0 \to K^0_S K^0_S$ plots for data (bottom plots), left to right: $M_{\rm bc}$ fits for the signal region for $D^0 \to K^0_S K^0_S$, sideband region 1 for $D^0 \to K^0_S K^0_S$ and sideband region 2 for $D^0 \to K^0_S K^0_S$. The sideband regions are shown in upper right plot. (Figure from reference, see text.)

reconstructed in both $\eta \to \gamma\gamma$ and $\eta \to \pi^+\pi^-\pi^0$ modes. Then combine the two fit yields from the different η decay modes according to the fit yield fractional error. The weighting factors for both $D_s^+ \to \pi^+\eta$ and $D_s^+ \to \pi^+\eta'$ are 0.65 for $\eta \to \gamma\gamma$ and 0.35 for $\eta \to \pi^+\pi^-\pi^0$. Apply the same weighting factors to the corresponding Cabibbo suppressed modes ($D_s^+ \to K^+\eta$ and $D_s^+ \to K^+\eta'$). Doing so guarantees cancellation of systematic errors between Cabibbo favored and Cabibbo suppressed modes. It also avoids a possible bias that could come from using the errors on the Cabibbo suppressed modes to determine the weighting factors for them.

Ratios of branching fractions are computed for each of the Cabibbo suppressed modes and are shown in Table 7 [28]. They are normalized with respect to the corresponding Cabibbo favored modes. The $D_s^+ \to K^+K^0_S$ mode is used to normalize the $D_s^+ \to K^+\pi^0$ mode. The upper limit for the unobserved mode $D_s^+ \to \pi^+\pi^0$, normalized with respect to $D_s^+ \to K^+K^0_S$, is also shown in Table 7 [28]. As a search for evidence of non-standard-model physics, CLEO-c has measured the CP asymmetries $\mathcal{A}_{CP} \equiv (\mathcal{B}_+ - \mathcal{B}_-)/(\mathcal{B}_+ + \mathcal{B}_-)$ for the four Cabibbo suppressed D_s decay modes. Results are given in the last column of Table 7 [28]. All asymmetries are consistent with zero.

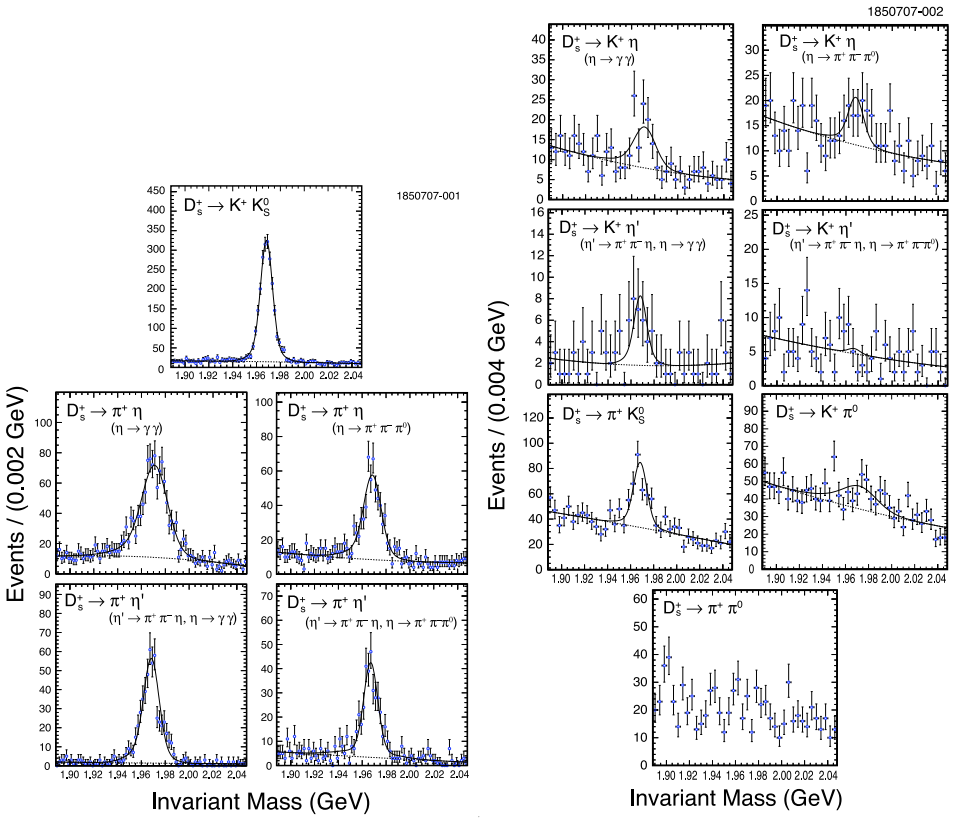

Fig. 11. $M(D_s)$ distributions for Cabibbo favored D_s modes (plots on left) and Cabibbo suppressed D_s modes (plots on right). The points are the data and the superimposed line is the fit (the dotted line is the fitted background). Also shown is the distribution for the isospin-forbidden decay $D_s^+ \to \pi^+\pi^0$. (Figure from reference, see text.)

Table 7. Ratios of branching fractions of Cabibbo suppressed modes to corresponding Cabibbo favored modes. Uncertainties are statistical and systematic, respectively. The last column is measured CP asymmetries in corresponding Cabibbo suppressed decay modes. Only statistical uncertainties are included. Systematic errors are negligible by comparison. (Table from reference, see text.)

Mode	$\mathcal{B}_S/\mathcal{B}_F(10^{-2})$	$\mathcal{A}_{CP}$ (%)
$\mathcal{B}(D_s^+ \to K^+\eta)$ / $\mathcal{B}(D_s^+ \to \pi^+\eta)$	$8.9 \pm 1.5 \pm 0.4$	-20 ± 18
$\mathcal{B}(D_s^+ \to K^+\eta')$ / $\mathcal{B}(D_s^+ \to \pi^+\eta')$	$4.2 \pm 1.3 \pm 0.3$	-17 ± 37
$\mathcal{B}(D_s^+ \to \pi^+K_S^0)$ / $\mathcal{B}(D_s^+ \to K^+K_S^0)$	$8.2 \pm 0.9 \pm 0.2$	$+27 \pm 11$
$\mathcal{B}(D_s^+ \to K^+\pi^0)$ / $\mathcal{B}(D_s^+ \to K^+K_S^0)$	$5.5 \pm 1.3 \pm 0.7$	$+2 \pm 29$
$\mathcal{B}(D_s^+ \to \pi^+\pi^0)$ / $\mathcal{B}(D_s^+ \to K^+K_S^0)$	< 4.1 (90% CL)	

7.5. *Doubly Cabibbo suppressed decay* $D^+ \to K^+\pi^0$

In addition to Cabibbo favored and singly Cabibbo suppressed decays, CLEO-c measured the doubly Cabibbo suppressed decay $D^+ \to K^+\pi^0$ by using 281 pb^{-1} of data

collected at the $\psi(3770)$ resonance [27], which has been observed by BABAR [61] using a sample of 124 fb^{-1} recorded at the $\Upsilon(4S)$. The unbinned maximum likelihood fit has been performed on the $M_{\rm bc}$ distributions to extract signal yields. The $M_{\rm bc}$ distributions for candidate combinations are shown in Fig. 12 [27]. The normalization mode $D^+ \to K^-\pi^+\pi^+$ is essentially background-free. The $D^+ \to \pi^+\pi^0$ mode background is well described by the distribution obtained from the ΔE sideband, as is that for the $D^+ \to K^+\pi^0$ mode. There is a clear peak in $D^+ \to K^+\pi^0$.

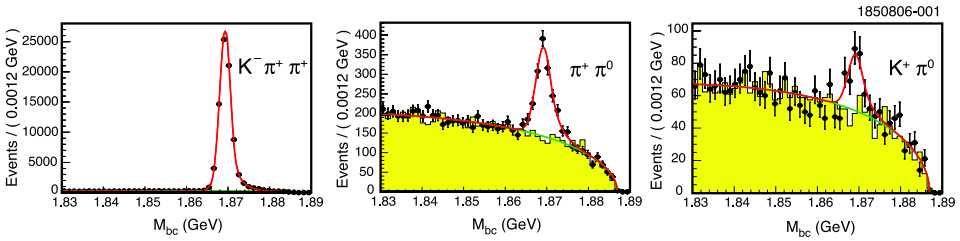

Fig. 12. $M_{\rm bc}$ distributions of $D^+ \to K^-\pi^+\pi^+$, $D^+ \to \pi^+\pi^0$ and $D^+ \to K^+\pi^0$. The points are obtained by selecting the ΔE signal region, the shaded histogram is from the ΔE sidebands, and the lines are the fit. (Figure from reference, see text.)

CLEO-c and BABAR find branching fractions in good agreement with each other, $\mathcal{B}(D^+ \to K^+\pi^0) = (2.28 \pm 0.36 \pm 0.15 \pm 0.08) \times 10^{-4}$ [27] and $\mathcal{B}(D^+ \to K^+\pi^0) = (2.52 \pm 0.46 \pm 0.24 \pm 0.08) \times 10^{-4}$ [61], respectively, and of comparable accuracy.

7.6. *Modes with K^0_L or K^0_S in the final states*

It has commonly been assumed that $\Gamma(D \to K^0_S X) = \Gamma(D \to K^0_L X)$. However, as pointed out by Bigi and Yamamoto [62] this is not generally true as for many D decays there are contributions from Cabibbo favored and Cabibbo suppressed decays that interfere and produce different rates to final states with K^0_S versus K^0_L. As an example consider $D^0 \to K^0_{S,L}\pi^0$. Contributions to these final states involve the Cabibbo favored decay $D^0 \to \bar{K}^0\pi^0$ as well as the doubly Cabibbo suppressed decay $D^0 \to K^0\pi^0$. However, we don't observe the K^0 and the $\bar{K}^0$ but rather the K^0_S and the K^0_L. As the amplitudes for $D^0 \to \bar{K}^0\pi^0$ and $D^0 \to K^0\pi^0$ interfere constructively to form the K^0_S final state, and destructively to form a K^0_L, we see a rate asymmetry between the K^0_L and K^0_S final states. Using $SU(3)$, and in particular the U-spin subgroup [63], one can predict the asymmetry in $D^0 \to K^0_{S,L}\pi^0$

$$R(D^0) = \frac{\Gamma(D^0 \to K^0_S\pi^0) - \Gamma(D^0 \to K^0_L\pi^0)}{\Gamma(D^0 \to K^0_S\pi^0) + \Gamma(D^0 \to K^0_L\pi^0)} \approx 2\tan^2\theta_C = 0.109 \pm 0.001.$$

Predictions for the asymmetry in charged D decays is more involved than for neutral D decays. because internal spectator diagrams contribute to both $D^+ \to \bar{K}^0\pi^+$

and $D^+ \to K^0\pi^+$, but external diagrams contribute to the former and annihilation diagrams contribute to the latter. D.-N. Gao, based on factorization, predicts [64] this asymmetry in $D^+ \to K^0_{S,L}\pi^+$

$$R(D^+) = \frac{\Gamma(D^+ \to K^0_S\pi^+) - \Gamma(D^+ \to K^0_L\pi^+)}{\Gamma(D^+ \to K^0_S\pi^+) + \Gamma(D^+ \to K^0_L\pi^+)}$$

to be in the range 0.035 to 0.044. Bhattacharya & Rosner, based on the diagrammatic approach, predict [67] this asymmetry to be $R(D^+) = -0.005 \pm 0.013$.

CLEO-c has measured the branching fractions for these decays by fully reconstructing $D \to K^0_S\pi$ decays and reconstructing $D \to K^0_L\pi$ decays using missing masses with a data sample of 281 pb^{-1} collected at the $\psi(3770)$ resonance [65]. The $D \to K^0_L\pi$ decays are illustrated in Fig. 13 [65]. Combined with the previous CLEO-c measurement for $D^+ \to K^0_S\pi^+$ [16], CLEO-c obtains the asymmetries in neutral and charged D decays

$$R(D^0) = 0.108 \pm 0.025 \pm 0.024$$
$$R(D^+) = 0.022 \pm 0.016 \pm 0.018,$$

which are in good agreenment with the predictions. There is no evidence for a significant asymmetry in the $D^+ \to K^0_{S,L}\pi^+$ mode.

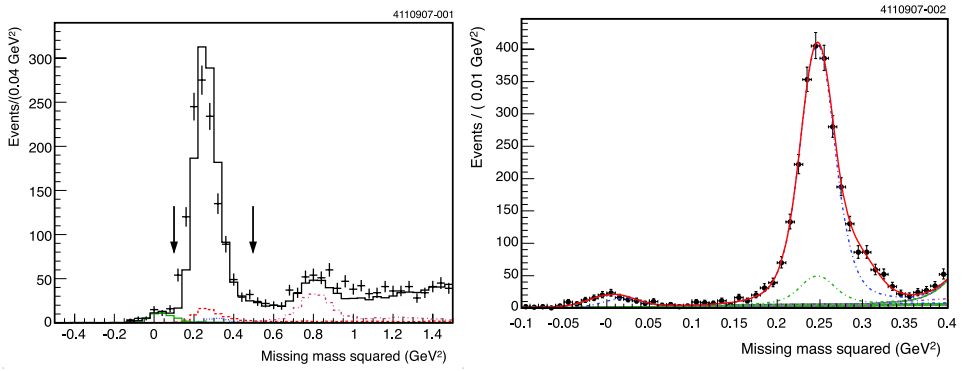

Fig. 13. Missing mass squared distribution, with all tag modes combined, for $D^0 \to X\pi^0$ (left plot) and $D^+ \to X\pi^+$ (right plot). (Figure from reference, see text.)

8. Measurements of *D* Meson Decays to Two Pseudoscaler Mesons

CLEO-c has published the results of branching fractions of D^0, D^+, and D^+_s decays to two pseudoscalars, based on an analysis of CLEO-c's full data set [31], with 818 pb^{-1} at $\psi(3770)$ corresponding to 3×10^6 $D^0\bar{D}^0$ pairs and 2.4×10^6 D^+D^- pairs; and 586 pb^{-1} at $E_{\rm cm} = 4170$ MeV corresponding to 5.4×10^5 $D^{*\pm}_s D^{\mp}_s$ pairs. Many of the resulting branching fraction measurements are more precise than the previous world average [22], and some decay modes have been seen for the first time.

8.1. $D \to PP$ branching fractions

There are many possible exclusive decays of charmed D mesons to a pair of mesons from the lowest-lying pseudoscalar meson nonet. The decay can be to any pair of K^+, K^-, π^+, π^-, η, η', π^0, K^0, or $\bar{K}^0$, with total charge 0 or ± 1. Measurements of the complete set of decays can be used to test flavor topology and $SU(3)$ predictions and to specify strong phases of decay amplitudes through triangle relations [66,67]. Moreover, many CP asymmetries (expected to be less than $\mathcal{O}(10^{-3})$ in the standard model) can be studied. In this analysis, CLEO-c reported all branching fractions for Cabibbo favored, singly Cabibbo suppressed, and doubly Cabibbo suppressed $D \to PP$ decays except modes involving K^0_L and except the doubly Cabibbo suppressed decay $D^0 \to K^+\pi^-$. The branching fractions have been normalized with respect to the Cabibbo favored D modes, $D^0 \to K^-\pi^+$ [16], $D^+ \to K^-\pi^+\pi^+$ [16], and $D_s^+ \to K^+K^0_S$ [49]. (More precisely, normalize the $D^0 \to PP$ decays with respect to the sum of the Cabibbo favored mode $D^0 \to K^-\pi^+$ and the doubly Cabibbo suppressed mode $D^0 \to K^+\pi^-$. The latter is 0.4% of the former.)

The $M_{\rm bc}$ distributions for the D^0 and D^+ candidate combinations are shown in Figs. 14 [31]. The resulting $M(D_s)$ distributions for D_s modes are shown in Fig. 15 [31]. For most of the $D \to PP$ modes, very clear signals are found in data. There is no significant evidence for $D^+ \to K^+\eta$, $D^+ \to K^+\eta'$, and $D_s^+ \to \pi^+\pi^0$ decays, and therefore upper limits are set on their branching fractions. The results are summarized in Table 8 [31].

The CP asymmetries are computed by using the separated yields and efficiencies for D and $\bar{D}$ events and are listed in the last column of Table 8 [31]. For D^0 vs. $\bar{D}^0$, the only asymmetry that can be measured is $K^-\pi^+$ vs. $K^+\pi^-$. That difference will contain a component from the difference in the doubly Cabibbo suppressed decays $D^0 \to K^+\pi^-$ vs. $\bar{D}^0 \to K^-\pi^+$, as well as the component from the favored decays $D^0 \to K^-\pi^+$ vs. $\bar{D}^0 \to K^+\pi^-$. CLEO-c does not separate these two possible asymmetries. Belle also searched for CP violation in the charged charmed meson decays $D^+_{(s)} \to K^0_S\pi^+$ and $D^+_{(s)} \to K^0_S K^+$ with a 637 fb^{-1} data sample [68]. No evidence for CP violation is observed.

8.2. *Flavor-topology amplitudes and relative phases*

The $SU(3)$ flavor symmetry has been shown useful in finding relative strong phases of amplitudes in $D \to PP$ decays [39,69,70]. The flavor-topology technique for analyzing charmed meson decays makes use of $SU(3)$ invariant amplitudes. Such kind of analysis has been done in Ref. 71, later repeated in Ref. 66, and recently updated in Ref. 67 and Ref. 72 with the new $D \to PP$ measurements from CLEO-c [31].

The decay amplitudes are expressed in terms of topological quark-flow diagrames; the diagrams used in this analysis are given in Fig. 16 [73]. The key amplitudes that describe the physics of Cabibbo-favored decays have been defined in Ref. 66, and include a color-favored tree (T), a color-suppressed tree (C), an exchange (E), and an annihilation (A) amplitude. The Cabibbo-favored (CF) amplitudes are pro-

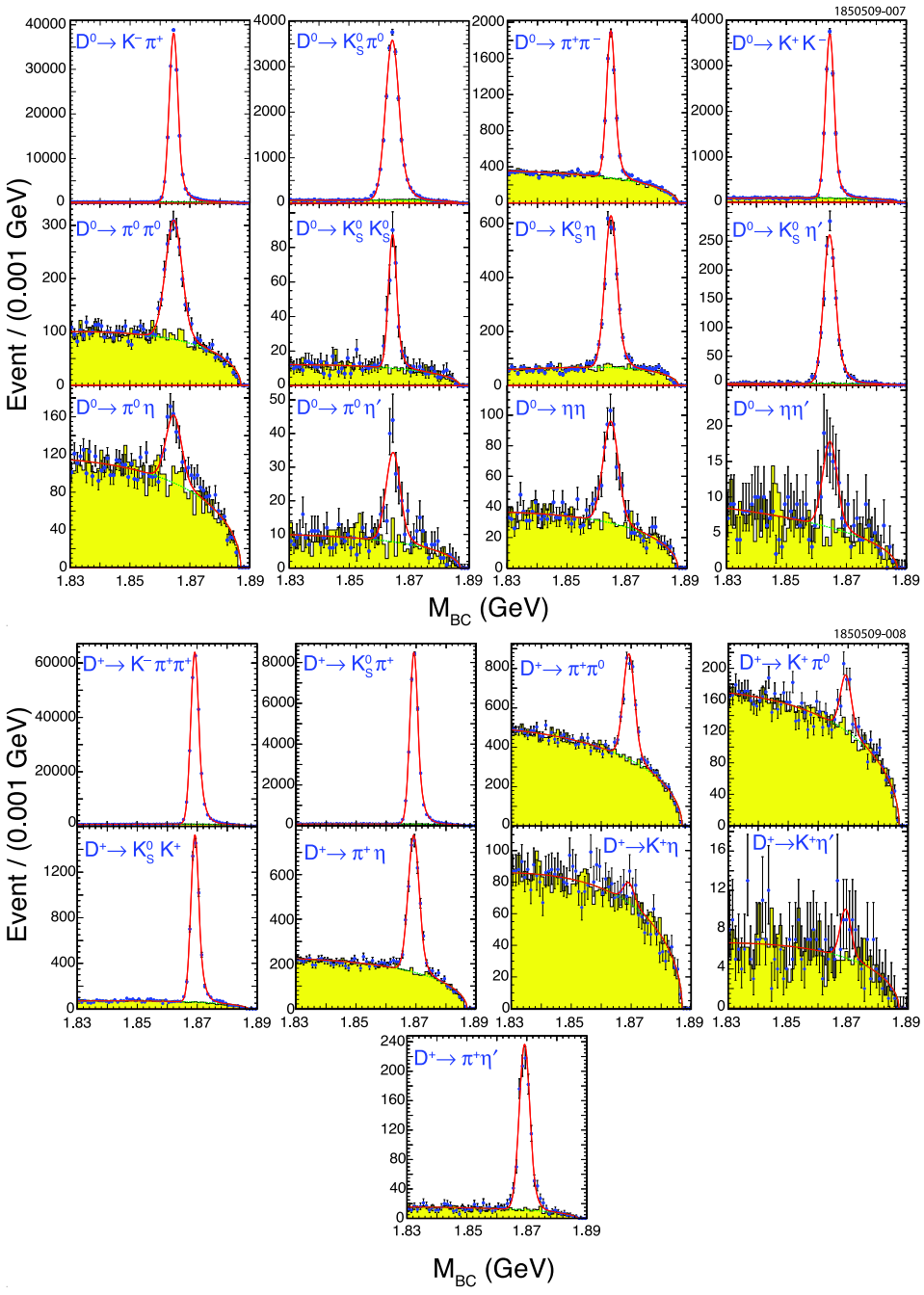

Fig. 14. $M_{\rm bc}$ distributions of D^0 and D^+ modes. For each distribution, the points are obtained from the ΔE signal region, the shaded histogram is from the ΔE sidebands, and the line is the fit. (Figure from reference, see text)

Table 8. Ratios of branching fractions to the corresponding normalization modes $D^0 \to K^-\pi^+$, $D^+ \to K^-\pi^+\pi^+$, and $D_s^+ \to K_S^0 K^+$; branching fractions results from $D \to PP$ analysis; and charge asymmetries $\mathcal{A}_{CP}$. Uncertainties are statistical error, systematic error, and the error from the input branching fractions of normalization modes. (Table from reference, see text.)

Mode	$\mathcal{B}_{\rm mode}/\mathcal{B}_{\rm Normalization}$ (%)	This result $\mathcal{B}$ (%)	$\mathcal{A}_{CP}$ (%)
$D^0 \to K^+K^-$	10.41 ± 0.11 ± 0.12	0.407 ± 0.004 ± 0.005 ± 0.008	
$D^0 \to K_S^0 K_S^0$	0.41 ± 0.04 ± 0.02	0.0160 ± 0.0017 ± 0.0008 ± 0.0003	
$D^0 \to \pi^+\pi^-$	3.70 ± 0.06 ± 0.09	0.145 ± 0.002 ± 0.004 ± 0.003	
$D^0 \to \pi^0\pi^0$	2.06 ± 0.07 ± 0.10	0.081 ± 0.003 ± 0.004 ± 0.002	
$D^0 \to K^-\pi^+ + \bar{D}^0 \to K^-\pi^+$	100	3.9058 external input [16]	0.5 ± 0.4 ± 0.9
$D^0 \to K_S^0\pi^0$	30.4 ± 0.3 ± 0.9	1.19 ± 0.01 ± 0.04 ± 0.02	
$D^0 \to K_S^0\eta$	12.3 ± 0.3 ± 0.7	0.481 ± 0.011 ± 0.026 ± 0.010	
$D^0 \to \pi^0\eta$	1.74 ± 0.15 ± 0.11	0.068 ± 0.006 ± 0.004 ± 0.001	
$D^0 \to K_S^0\eta'$	24.3 ± 0.8 ± 1.1	0.95 ± 0.03 ± 0.04 ± 0.02	
$D^0 \to \pi^0\eta'$	2.3 ± 0.3 ± 0.2	0.091 ± 0.011 ± 0.006 ± 0.002	
$D^0 \to \eta\eta$	4.3 ± 0.3 ± 0.4	0.167 ± 0.011 ± 0.014 ± 0.003	
$D^0 \to \eta\eta'$	2.7 ± 0.6 ± 0.3	0.105 ± 0.024 ± 0.010 ± 0.002	
$D^+ \to K^-\pi^+\pi^+$	100	9.1400 external input [16]	-0.1 ± 0.4 ± 0.9
$D^+ \to K_S^0 K^+$	3.35 ± 0.06 ± 0.07	0.306 ± 0.005 ± 0.007 ± 0.007	-0.2 ± 1.5 ± 0.9
$D^+ \to \pi^+\pi^0$	1.29 ± 0.04 ± 0.05	0.118 ± 0.003 ± 0.005 ± 0.003	2.9 ± 2.9 ± 0.3
$D^+ \to K_S^0\pi^+$	16.82 ± 0.12 ± 0.37	1.537 ± 0.011 ± 0.034 ± 0.033	-1.3 ± 0.7 ± 0.3
$D^+ \to K^+\pi^0$	0.19 ± 0.02 ± 0.01	0.0172 ± 0.0018 ± 0.0007 ± 0.0004	-3.5 ± 10.7 ± 0.9
$D^+ \to K^+\eta$	< 0.15 (90% C.L.)	< 0.013 (90% C.L.)	
$D^+ \to \pi^+\eta$	3.87 ± 0.09 ± 0.19	0.354 ± 0.008 ± 0.018 ± 0.008	-2.0 ± 2.3 ± 0.3
$D^+ \to K^+\eta'$	< 0.20 (90% C.L.)	< 0.019 (90% C.L.)	
$D^+ \to \pi^+\eta'$	5.12 ± 0.17 ± 0.25	0.468 ± 0.016 ± 0.023 ± 0.010	-4.0 ± 3.4 ± 0.3
$D_s^+ \to K_S^0 K^+$	100	1.4900 external input [49]	4.7 ± 1.8 ± 0.9
$D_s^+ \to \pi^+\pi^0$	< 2.3 (90% C.L.)	< 0.037 (90% C.L.)	
$D_s^+ \to K_S^0\pi^+$	8.5 ± 0.7 ± 0.2	0.126 ± 0.011 ± 0.003 ± 0.007	16.3 ± 7.3 ± 0.3
$D_s^+ \to K^+\pi^0$	4.2 ± 1.4 ± 0.2	0.062 ± 0.022 ± 0.004 ± 0.004	-26.6 ± 23.8 ± 0.9
$D_s^+ \to K^+\eta$	11.8 ± 2.2 ± 0.6	0.176 ± 0.033 ± 0.009 ± 0.010	9.3 ± 15.2 ± 0.9
$D_s^+ \to \pi^+\eta$	123.6 ± 4.3 ± 6.3	1.84 ± 0.06 ± 0.09 ± 0.11	-4.6 ± 2.9 ± 0.3
$D_s^+ \to K^+\eta'$	11.8 ± 3.6 ± 0.7	0.18 ± 0.05 ± 0.01 ± 0.01	6.0 ± 18.9 ± 0.9
$D_s^+ \to \pi^+\eta'$	265.4 ± 8.8 ± 13.9	3.95 ± 0.13 ± 0.21 ± 0.23	-6.1 ± 3.0 ± 0.3

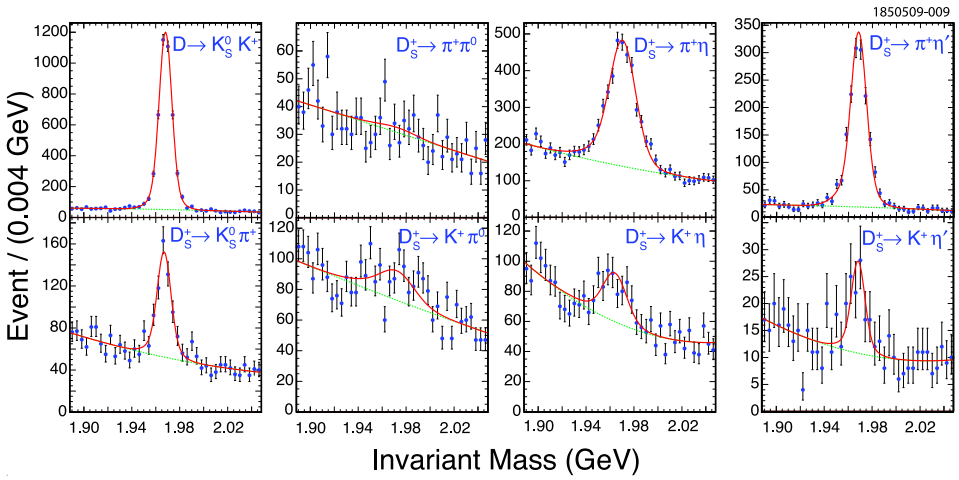

Fig. 15. $M(D_s)$ distributions for D_s modes. For each distribution, the points are the data and the superimposed line is the fit (the dotted line is the fitted background). (Figure from reference, see text.)

portional to the product $V_{ud}V_{cs}$, the singly Cabibbo-suppressed amplitudes are proportional to $V_{us}V_{cs}$ or $V_{ud}V_{cd}$, and the doubly Cabibbo-suppressed amplitudes are proportional to $V_{us}V_{cd}$. The relative hierarchy of these amplitudes in terms of the Wolfenstein parameter $\lambda = \tan\theta_C = 0.2317$ [67] is $1 : \lambda : -\lambda : -\lambda^2$, where θ_C is the Cabibbo angle.

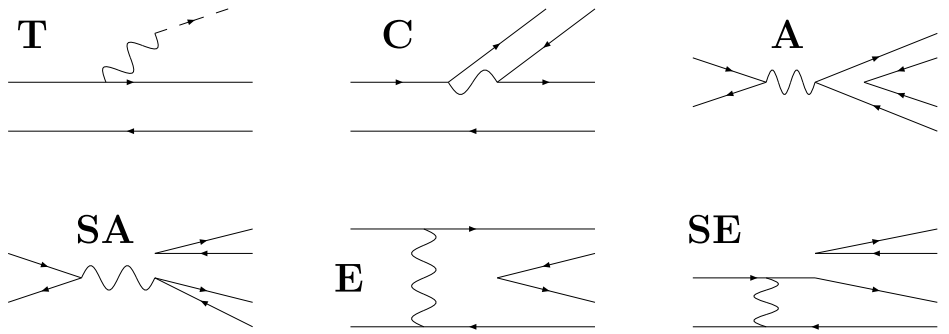

Fig. 16. Quark flow diagrams, from top-left to bottom-right, **T**ree, **C**olour-suppressed tree, **A**nnihiliation, **S**inglet-emission with **A**nnihilation, **E**xchange, and **S**inglet-emission with **E**xchange. (Figure from reference, see text.)

Table 9 [67] lists the corresponding representations of the Cabibbo-favored decay amplitudes as functions of the octet-singlet mixing angle θ_η. The singlet contributions to these decays are deemed to be negligible. The table compares the measured

branching fractions with the result from the best-fit to the quark flow diagram formalism for two solutions. One where the θ_η is fixed to $\theta_\eta = \arcsin(1/3) = 19.5°$, and another, where the θ_η is allowed to vary, giving $\theta_\eta = 11.7°$. The latter case has as many parameters as there are CF decay rates used as constraints, so the agreement between the prediction from the formalism given in the fifth column of Table 9 [67], and the measured CF amplitudes given in the second, is exact by construction. A further solution, with $|T| < |C|$, is also discussed in Ref. 67. Fig. 17 [67] shows the constructions of the amplitudes from the rates given in Table 9 [67] for these two cases. The corresponding amplitudes, in the case for $\theta_\eta = 11.7°$, are:

$$\begin{aligned} T &= 3.003 \pm 0.023, \\ C &= (2.565 \pm 0.030) \exp\left[i(-152.11 \pm 0.57)^\circ\right], \\ E &= (1.372 \pm 0.036) \exp\left[i(123.62 \pm 1.25)^\circ\right], \\ A &= (0.452 \pm 0.058) \exp\left[i(19^{+15}_{-14})^\circ\right]; \end{aligned}$$

and in the case for $\theta_\eta = \arcsin(1/3) = 19.5°$ are:

$$\begin{aligned} T &= 2.927 \pm 0.022, \\ C &= (2.337 \pm 0.027) \exp\left[i(-151.66 \pm 0.63)^\circ\right], \\ E &= (1.573 \pm 0.032) \exp\left[i(120.56 \pm 1.03)^\circ\right], \\ A &= (0.33 \pm 0.14) \exp\left[i(70.47 \pm 10.90)^\circ\right]. \end{aligned}$$

These results are then used to predict the decay amplitudes of singly Cabibbo suppressed (SCS) and doubly Cabibbo suppressed (DCS) two body decays, which are shown in Table 10 [67] and Table 11 [67] respectively. The predictions for decays involving kaons and pions only are mostly in reasonable agreement with measurements although the approach considerably overestimates $\mathcal{B}(D^0 \to \pi^+\pi^-)$ and underestimates $\mathcal{B}(D^0 \to K^+K^-)$.

Table 9. Branching ratios and invariant amplitudes for Cabibbo-favored decays of charmed mesons to a pair of pseudoscalars with 2 different values of θ_η. ($\phi_1 = 45° - \frac{\phi_2}{2}$ and $\phi_2 = 19.5°$.) (Table from reference, see text.)

Meson	Decay mode	$\mathcal{B}$ [31] (%)	Rep.	Predicted $\mathcal{B}$(%) $\theta_\eta = 11.7°$	$\theta_\eta = 19.5°$
D^0	$K^-\pi^+$	3.891±0.077	$T + E$	3.891	3.905
	$\overline{K}^0\pi^0$	2.380±0.092	$(C - E)/\sqrt{2}$	2.380	2.347
	$\overline{K}^0\eta$	0.962±0.060	$\frac{C}{\sqrt{2}}\sin(\theta_\eta + \phi_1) - \frac{\sqrt{3}E}{\sqrt{2}}\cos(\theta_\eta + 2\phi_1)$	0.962	1.002
	$\overline{K}^0\eta'$	1.900±0.108	$-\frac{C}{\sqrt{2}}\cos(\theta_\eta + \phi_1) - \frac{\sqrt{3}E}{\sqrt{2}}\sin(\theta_\eta + 2\phi_1)$	1.900	1.920
D^+	$\overline{K}^0\pi^+$	3.074±0.097	$C + T$	3.074	3.090
D_s^+	$\overline{K}^0K^+$	2.98±0.17	$C + A$	2.980	2.939
	$\pi^+\eta$	1.84±0.15	$T\cos(\theta_\eta + \phi_1) - \sqrt{2}A\sin(\theta_\eta + \phi_1)$	1.840	1.810
	$\pi^+\eta'$	3.95±0.34	$T\sin(\theta_\eta + \phi_1) + \sqrt{2}A\cos(\theta_\eta + \phi_1)$	3.950	3.603

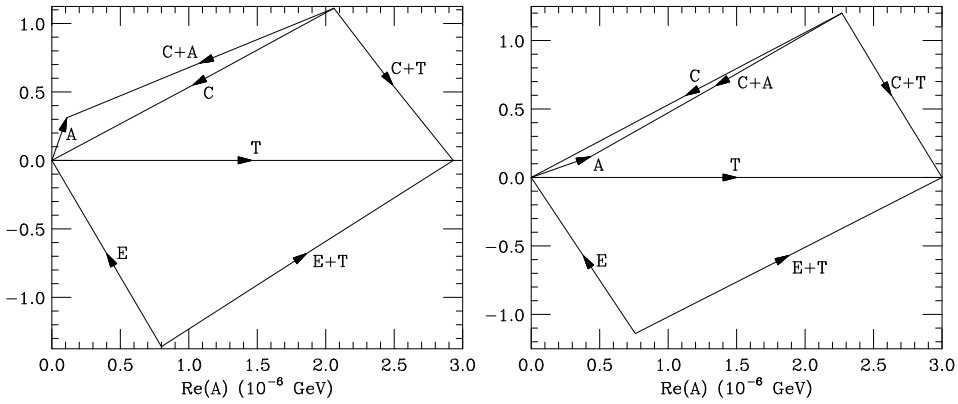

Fig. 17. Construction of Cabibbo-favored amplitudes from observed processes using a least χ^2 fit. The sides $C+T$, $C+A$, and $E+T$ correspond to measured processes; the magnitudes of other amplitudes listed in Table 9 are also needed to specify T, C, E, and A. These figures correspond to the $|T| > |C|$ solution. Left: θ_η fixed at $\arcsin(1/3) = 19.5^\circ$ with $\chi^2 = 1.79$ for 1 degree of freedom. Right: exact solution with $\theta_\eta = 11.7^\circ$ and $\chi^2 = 0$. (Figure from reference, see text.)

Table 10. Branching ratios and invariant amplitudes for singly Cabibbo-suppressed decays of charmed mesons to pions and kaons. (Table from reference, see text.)

Meson	Decay mode	$\mathcal{B}$[31] (10^{-3})	p^* (MeV/c)	$\lvert\mathcal{A}\rvert$ (10^{-7}GeV)	Rep.	Predicted $\mathcal{B}$ (10^{-3}) $\lvert T\rvert < \lvert C\rvert$	$\lvert T\rvert > \lvert C\rvert$
D^0	$\pi^+\pi^-$	1.45 ± 0.05	921.9	4.70 ± 0.08	$-(T' + E')$	2.24	2.24
	$\pi^0\pi^0$	0.81 ± 0.05	922.6	3.51 ± 0.11	$-(C' - E')/\sqrt{2}$	1.36	1.35
	K^+K^-	4.07 ± 0.10	791.0	8.49 ± 0.10	$(T' + E')$	1.92	1.93
	$K^0\overline{K}^0$	0.32 ± 0.02	788.5	2.39 ± 0.14	0	0	0
D^+	$\pi^+\pi^0$	1.18 ± 0.06	924.7	2.66 ± 0.07	$-(T' + C')/\sqrt{2}$	0.88	0.89
	$K^+\overline{K}^0$	6.12 ± 0.22	792.6	6.55 ± 0.12	$(T' - A')$	0.73	6.15
D_s^+	π^+K^0	2.52 ± 0.27	915.7	5.94 ± 0.32	$-(T' - A')$	0.37	3.08
	π^0K^+	0.62 ± 0.23	917.1	2.94 ± 0.55	$-(C' + A')/\sqrt{2}$	0.86	0.85

For singly Cabibbo-suppressed decays involving η and η', there are indications for a non-negligible contribution from the singlet annihilation diagrams. The "disconnected" flavor-singlet diagrams SE' and SA' [71] are required. Table 12 [67] shows the representations of these amplitudes as a function of θ_η. A plotting technique [39,66,67,69,70] is used to determine SE' and SA' as illustrated in Fig. 18 [67]. The detailed description of this approach and its result can be found in Ref. 67.

Table 11. Branching ratios and amplitudes for doubly Cabibbo-suppressed decays of D^0, D^+ and D_s^+. (Table from reference, see text.)

Meson	Decay mode	$\mathcal{B}^{31}$ (10^{-4})	p^* (MeV/c)	Representation	Predicted $\mathcal{B}$ $\theta_\eta = 11.7°$
D^0	$K^+\pi^-$	1.45 ± 0.04	861.1	$\tilde{T} + \tilde{E}$	1.12
	$K^0\pi^0$		860.4	$(\tilde{C} - \tilde{E})/\sqrt{2}$	0.69
	$K^0\eta$		771.9	$\frac{\tilde{C}}{\sqrt{2}}\sin(\theta_\eta + \phi_1) - \frac{\sqrt{3}\tilde{E}}{\sqrt{2}}\cos(\theta_\eta + 2\phi_1)$	0.28
	$K^0\eta'$		564.9	$-\frac{\tilde{C}}{\sqrt{2}}\cos(\theta_\eta + \phi_1) - \frac{\sqrt{3}\tilde{E}}{\sqrt{2}}\sin(\theta_\eta + 2\phi_1)$	0.55
D^+	$K^0\pi^+$		862.6	$\tilde{C} + \tilde{A}$	2.01
	$K^+\pi^0$	1.72 ± 0.19	864.0	$(\tilde{T} - \tilde{A})/\sqrt{2}$	1.49
	$K^+\eta$	< 1.3	775.8	$-\frac{\tilde{T}}{\sqrt{2}}\sin(\theta_\eta + \phi_1) - \frac{\sqrt{3}\tilde{A}}{\sqrt{2}}\cos(\theta_\eta + 2\phi_1)$	1.06
	$K^+\eta'$	< 1.8	570.8	$\frac{\tilde{T}}{\sqrt{2}}\cos(\theta_\eta + \phi_1) + \frac{\sqrt{3}\tilde{A}}{\sqrt{2}}\sin(\theta_\eta + 2\phi_1)$	1.16
D_s^+	K^0K^+		850.3	$\tilde{T} + \tilde{C}$	0.38

Table 12. Representations for singly Cabibbo-suppressed decays of D^0, D^+ and D_s^+ involving η and η' for an arbitrary $\eta - \eta'$ mixing angle θ_η. ($\phi_1 = 45° - \frac{\phi_2}{2}$ and $\phi_2 = 19.5°$.) (Table from reference, see text.)

Meson	Decay mode	Representation
D^0	$\pi^0\eta$	$\frac{C'}{\sqrt{2}}\cos(\theta_\eta + \phi_1) - E'\ \sin(\theta_\eta + \phi_1) - \frac{\sqrt{3}\ SE'}{\sqrt{2}}\ \sin\theta_\eta$
	$\pi^0\eta'$	$\frac{C'}{\sqrt{2}}\sin(\theta_\eta + \phi_1) + E'\ \cos(\theta_\eta + \phi_1) + \frac{\sqrt{3}\ SE'}{\sqrt{2}}\ \cos\theta_\eta$
	$\eta\eta$	$\frac{\sqrt{3}\ C'}{\sqrt{2}}\cos\theta_\eta\ \sin(\theta_\eta + \phi_1) - \frac{3\ E'}{\sqrt{2}}\cos\theta_\eta\ \cos(\theta_\eta + 2\phi_1) + \frac{3\ SE'}{2}\sin(2\theta_\eta)$
	$\eta\eta'$	$-\frac{\sqrt{3}\ C'}{2}\cos(2\theta_\eta + \phi_1) + \frac{3\ E'}{2}\sin(2\theta_\eta + 2\phi_1) - \frac{3\ SE'}{\sqrt{2}}\cos(2\theta_\eta)$
D^+	$\pi^+\eta$	$\frac{T'}{\sqrt{2}}\sin(\theta_\eta + \phi_1) + \frac{\sqrt{3}\ C'}{\sqrt{2}}\cos\theta_\eta + \sqrt{2}\ A'\ \sin(\theta_\eta + \phi_1) + \sqrt{3}\ SA'\ \sin\theta_\eta$
	$\pi^+\eta'$	$-\frac{T'}{\sqrt{2}}\cos(\theta_\eta + \phi_1) + \frac{\sqrt{3}\ C'}{\sqrt{2}}\sin\theta_\eta - \sqrt{2}\ A'\ \cos(\theta_\eta + \phi_1) - \sqrt{3}\ SA'\ \cos\theta_\eta$
D_s^+	$K^+\eta$	$T'\ \cos(\theta_\eta + \phi_1) + \frac{\sqrt{3}\ C'}{\sqrt{2}}\cos\theta_\eta\ +\ \frac{\sqrt{3}\ A'}{\sqrt{2}}\cos(\theta_\eta + 2\phi_1) - \sqrt{3}\ SA'\ \sin\theta_\eta$
	$K^+\eta'$	$T'\ \sin(\theta_\eta + \phi_1) + \frac{\sqrt{3}\ C'}{\sqrt{2}}\sin\theta_\eta\ -\ \frac{\sqrt{3}\ A'}{\sqrt{2}}\ \sin(\theta_\eta + 2\phi_1) + \sqrt{3}\ SA'\ \cos\theta_\eta$

9. Inclusive D^0, D^+ and D_s Decays

9.1. *Inclusive mesurements of η, η' and ϕ production*

CLEO-c utilizes 281 pb^{-1} of $\psi(3770)$ data for D^0 and D^+ decays and 195 pb^{-1} of data at $E_{\rm cm} = 4170$ MeV for D_s^+ decays to measure branching fractions for inclusive D^0, D^+, and D_s^+ decays to ηX, $\eta' X$, and ϕX [74]. The fully reconstructed D candidate in one of the favorable modes [74] is used as a tag for event, then search for η, η' and ϕ in the decay products from the other D. The distributions in $M(\eta') - M(\eta)$, the difference between the invariant masses of the η' candidate and the η candidate in its decay chain, are used to determine the inclusive $\eta' X$ signal yields as illustrated in Fig 19 [74,75]. Similar distributions for $M(\eta)$ and $M(\phi)$ are

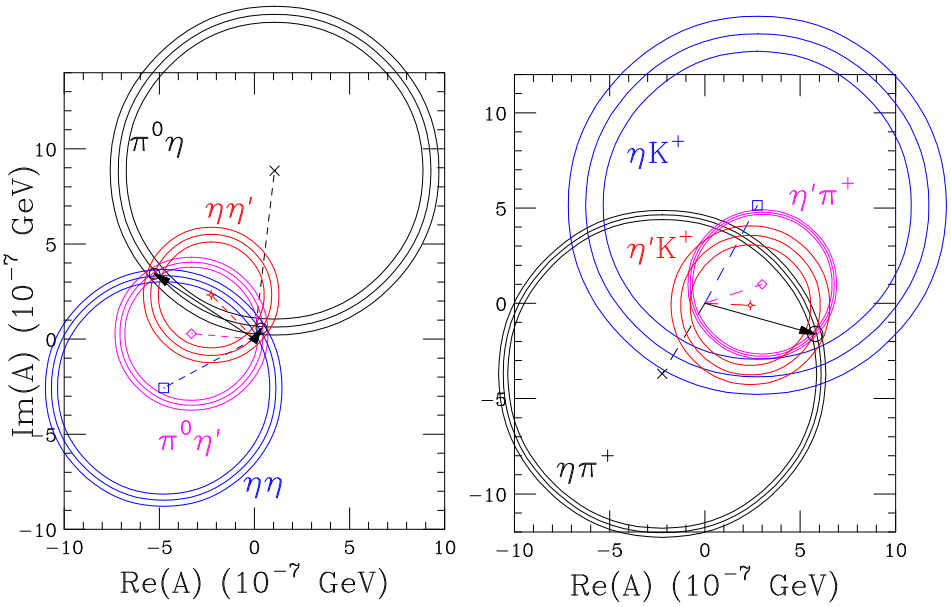

Fig. 18. Determination of the disconnected singlet annihilation amplitudes SE' (left) and SA' (right) from SCS charmed meson decays involving η and η' in the solutions with $|T| > |C|$ and $\theta_\eta = 19.5°$. Left: D^0 decays to final states as shown; right: D^+ or D_s^+ decays to final states as shown. The small black circles show the solution regions. Arrows pointing to them denote the complex amplitudes $-SE'$ (left) and $-SA'$ (right). (Figure from reference, see text.)

used to determine the signal yields for ηX and ϕX. Fitted yields from ΔE sidebands are then subtracted from the signal yields. The results are summarized in Table 13. Due to the $s\bar{s}$ content of η, η', and ϕ, as expected, the inclusive branching fractions for D_s decays to these particles are much higher than the branching fractions for corresponding D^0 and D^+ decays.

Table 13. Summary of inclusive branching ratio results. (Table from reference, see text.)

Mode	$\mathcal{B}(D^0)$ (%)	$\mathcal{B}(D^+)$ (%)	$\mathcal{B}(D_s^+)$ (%)
ηX	$9.5 \pm 0.4 \pm 0.8$	$6.3 \pm 0.5 \pm 0.5$	$23.5 \pm 3.1 \pm 2.0$
$\eta' X$	$2.48 \pm 0.17 \pm 0.21$	$1.04 \pm 0.16 \pm 0.09$	$8.7 \pm 1.9 \pm 0.8$
ϕX	$1.05 \pm 0.08 \pm 0.07$	$1.03 \pm 0.10 \pm 0.07$	$16.1 \pm 1.2 \pm 1.1$

9.2. *Inclusive hadron yields from D_s^+ decays*

Using 586 pb^{-1} of data collected near the $D_s^{*\pm}D_s^{\mp}$ peak production energy $E_{\rm cm} =$ 4170 MeV, CLEO-c published the measurements of the inclusive yields of D_s^+ decays to K^+X, K^-X, K_S^0X, π^+X, π^-X, π^0X, ηX, $\eta' X$, ϕX, ωX and $f_0(980)X$, and also

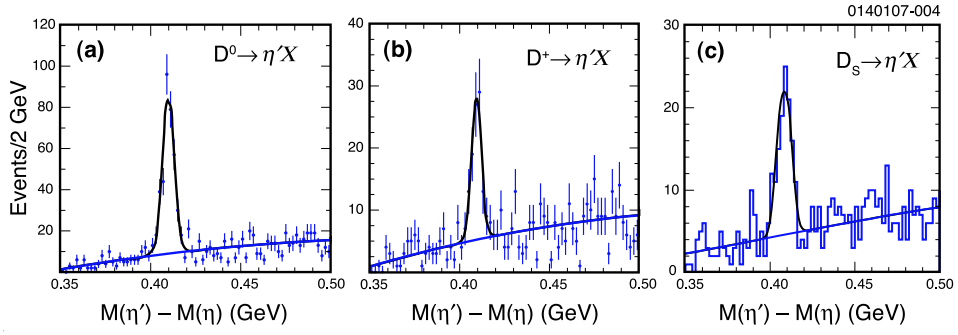

Fig. 19. The distributions of $M(\eta') - M(\eta)$, the difference between the invariant masses of the η' candidate and the η candidate: (a) candidates for $D^0 \to \eta' X$, (b) candidates for $D^+ \to \eta' X$, and (c) candidates for $D_s^+ \to \eta' X$. (Figure from reference, see text.)

decays into pairs of kaons, $D_s^+ \to K\bar{K}X$ [30]. In addition to providing an improved Monte Carlo decay table, the measurements of many inclusive yields from D_s^+ decays allow some comparisons with expectations [76].

The events used in this study are $e^+e^- \to D_s^{*\pm}D_s^{\mp}$, followed by $D^* \to D_s\gamma$. Single tag (ST) events are selected by fully reconstructing a D_s^- meson, either primary or from D_s^{*-} decay, which is called as a tag, in one of the following three two-body hadronic decay modes: $D_s^- \to K_S^0 K^-$, $D_s^- \to \phi\pi^-$ and $D_s^- \to K^{*0}K^-$. Then locate the γ from D_s^* decay. Everything else in the event is from the decay of the other D_s^+. CLEO-c looks at those "pieces" to obtain the inclusive yields. Mention of a specific mode implies the use of the charge conjugate mode as well. Thus such as, when refer to the inclusive process $D_s^+ \to \pi^+ X$, it implicitly is including the charge conjugate $D_s^- \to \pi^- X$, but not including $D_s^+ \to \pi^- X$ or $D_s^- \to \pi^+ X$. The invariant mass distributions of D_s tag candidates for each tag mode are shown Fig. 20 [30]. Total 18586 ± 163 ST events are obtained for this analysis.

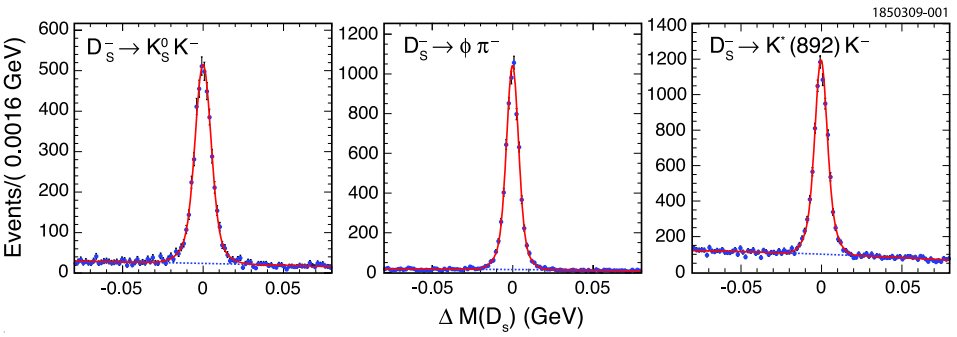

Fig. 20. The mass difference $\Delta M(D_s) \equiv M(D_s) - m_{D_s}$ distributions in each tag mode. Fit the $\Delta M(D_s)$ distribution (points) to the sum (solid curve) of signal (double-Gaussian) plus background (second degree polynomial, dashed curve) functions. (Figure from reference, see text.)

The inclusive yields are listed in Table 14 [30]. As a check for K^0_S modes, CLEO-c has measured the inclusive yields for the decay $D^+_s \to K^0_L X$ without directly detecting the K^0_L. Instead, reconstruct all particles in the event except the single K^0_L and infer the presence of a K^0_L from the missing four-momentum. The signal is a peak in the missing mass squared distribution at the K^0_L mass squared. In addition to the measurements of single particle inclusive yields, CLEO-c also measured the inclusive yields of D^+_s mesons into two kaons. A theoretical study [76] of inclusive branching fractions in D^+_s decays has been done to compare with experimental results [30], by augmenting the extensive list of known processes with estimates for unobserved modes based on isospin arguments, particularly those employing a statistical model [77,78,79].

Table 14. D_s inclusive yield results. Uncertainties are statistical and systematic, respectively. The inclusive K^0_L results are only used as a check for K^0_S. The $D^+_s \to K^0_L X$ yield requires a correction before comparing with the $D^+_s \to K^0_S X$ yield. Previous PDG averages are shown in the last column, when available, for non-CLEO measurements. (Table from reference, see text.)

Mode	Yield(%)	K^0_L Mode	Yield(%)	$\mathcal{B}$(PDG)(%)
$D^+_s \to \pi^+ X$	$119.3 \pm 1.2 \pm 0.7$			
$D^+_s \to \pi^- X$	$43.2 \pm 0.9 \pm 0.3$			
$D^+_s \to \pi^0 X$	$123.4 \pm 3.8 \pm 5.3$			
$D^+_s \to K^+ X$	$28.9 \pm 0.6 \pm 0.3$			$20\ ^{+18}_{-14}$
$D^+_s \to K^- X$	$18.7 \pm 0.5 \pm 0.2$			$13\ ^{+14}_{-12}$
$D^+_s \to \eta X$	$29.9 \pm 2.2 \pm 1.7$			
$D^+_s \to \eta' X$	$11.7 \pm 1.7 \pm 0.7$			
$D^+_s \to \phi X$	$15.7 \pm 0.8 \pm 0.6$			
$D^+_s \to \omega X$	$6.1 \pm 1.4 \pm 0.3$			
$D^+_s \to f_0(980) X$				
$\to (\pi^+\pi^- X)$	$< 1.3\%$ (90% CL)			
$D^+_s \to K^0_S X$	$19.0 \pm 1.0 \pm 0.4$	$K^0_L X$	15.6 ± 2.0	20 ± 14
$D^+_s \to K^0_S K^0_S X$	$1.7 \pm 0.3 \pm 0.1$	$K^0_L K^0_S X$	5.0 ± 1.0	
$D^+_s \to K^0_S K^+ X$	$5.8 \pm 0.5 \pm 0.1$	$K^0_L K^+ X$	5.2 ± 0.7	
$D^+_s \to K^0_S K^- X$	$1.9 \pm 0.4 \pm 0.1$	$K^0_L K^- X$	1.9 ± 0.3	
$D^+_s \to K^+ K^- X$	$15.8 \pm 0.6 \pm 0.3$			
$D^+_s \to K^+ K^+ X$	$< 0.26\%$ (90% CL)			
$D^+_s \to K^- K^- X$	$< 0.06\%$ (90% CL)			

9.3. *Overview of D^+_s decays*

The quark-level diagrams contributing to D^+_s decay are shown in Fig. 21 [30] and classified as $s\bar{s}$ (as would come from Fig. 21(a)), $\bar{s}$ (Fig. 21(b)), $s\bar{s}\bar{s}$ (Fig. 21(c)), $\bar{s}\bar{s}$ (Fig. 21(d)), and "no strange quarks" (Fig. 21(e) and Fig. 21(f)). The $s\bar{s}$ final state is Cabibbo-favored. The $\bar{s}$ and $s\bar{s}\bar{s}$ final states are singly Cabibbo-suppressed, the $\bar{s}\bar{s}$ final state is doubly Cabibbo-suppressed, and the "no strange quarks" final state arises from short-range (Fig. 21(e)) and long-range (Fig. 21(f)) annihilation

diagrams (While Fig. 21(f) shows the $s\bar{s}$ annihilating into gluons, here also include its rescattering into $u\bar{u}$ or $d\bar{d}$).

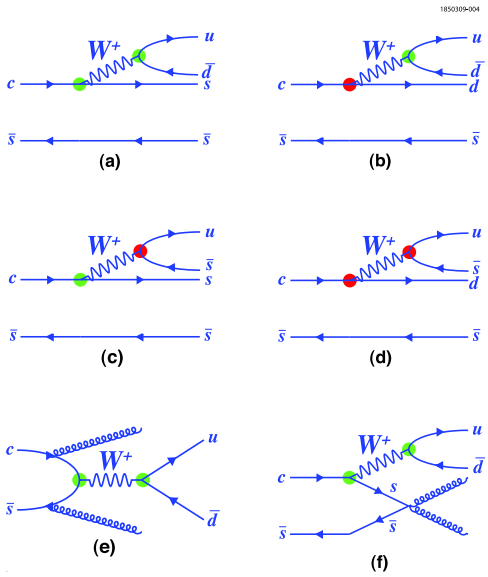

Fig. 21. The typical Feynman diagrams of D_s^+ decays: (a) Cabibbo-favored decay, (b) singly Cabibbo-suppressed decay, (c) singly Cabibbo-suppressed decay, (d) doubly Cabibbo-suppressed decay, (e) short-range annihilation decay, (f) long-range annihilation decay. (Figure from reference, see text.)

The $s\bar{s}$ final state can hadronize as $K\bar{K}X$, but also as ηX, $\eta' X$, or ϕX. The $\bar{s}$ final state will hadronize as KX. The $s\bar{s}\bar{s}$ final state in principle can hadronize as $KK\bar{K}X$, but there will be limited phase space for this, so $K\eta X$, $K\eta' X$, $K\phi X$ are probably as likely, if not more so. The $\bar{s}\bar{s}$ final state will hadronize as KKX, but being doubly Cabibbo-suppressed, can probably be ignored.

CLEO-c has performed a global fit to the measurements of inclusive yields from D_s^+ decays [30]. The χ^2 is defined as

$$\chi^2 = \left(\frac{\mathrm{Y}_\eta - \{\mathcal{B}(\eta)+\mathcal{B}(\eta\bar{s})+\mathcal{B}(\eta'\to\eta X)\times[\mathcal{B}(\eta')+\mathcal{B}(\eta'\bar{s})+f_2\times\mathcal{B}(\bar{s})]+\mathcal{B}(\text{extra }\eta)+f_1\times\mathcal{B}(\bar{s})\}}{\delta_{\mathrm{Y}_\eta}}\right)^2 +$$
$$\left(\frac{\mathrm{Y}_{\eta'} - [\mathcal{B}(\eta')+\mathcal{B}(\eta'\bar{s})+f_2\times\mathcal{B}(\bar{s})]}{\delta_{\mathrm{Y}_{\eta'}}}\right)^2 +$$
$$\left(\frac{\mathrm{Y}_\phi - [\mathcal{B}(\phi)+\mathcal{B}(\phi\bar{s})]}{\delta_{\mathrm{Y}_\phi}}\right)^2 +$$
$$\left(\frac{\mathrm{Y}_{KK} - \{\mathcal{B}(K\bar{K})+\mathcal{B}(K\bar{K}\bar{s})+\mathcal{B}(\phi\to K\bar{K})\times[\mathcal{B}(\phi)+\mathcal{B}(\phi\bar{s})]+\mathcal{B}(\bar{s}\bar{s})\}}{\delta_{\mathrm{Y}_{KK}}}\right)^2 +$$
$$\left(\frac{\mathrm{Y}_K - \{2\times[\mathcal{B}(K\bar{K})+\mathcal{B}(K\bar{K}\bar{s})]+2\times\mathcal{B}(\phi\to K\bar{K})\times[\mathcal{B}(\phi)+\mathcal{B}(\phi\bar{s})]+\mathcal{B}(s\bar{s}\bar{s})+\mathcal{B}(\bar{s})+2\times\mathcal{B}(\bar{s}\bar{s})\}}{\delta_{\mathrm{Y}_K}}\right)^2 \tag{8}$$

Here Y_i is the central value of a measurement, and δ_{Y_i} is the error on that mea-

surement. The detailed description of this global fit can be found in Ref. 30. Fit results are given in Table 15 [30].

Table 15. Results from the global fit. The central values of parameters are listed in second column. The errors: δ_1 is statistical uncertainty, δ_2 is from phase space factor $C_1 = 1.25 \pm 0.25$, δ_3 is from phase space factor $C_2 = 0.75 \pm 0.25$, δ_4 is from $f_1 + f_2 = 0.5 \pm 0.5$, and δ_5 is from the $\mathcal{B}(\text{extra } \eta) = (6.0 \pm 3.9)\%$. (Table from reference, see text.)

		Error(%)				
Parameter	Value(%)	δ_1	δ_2	δ_3	δ_4	δ_5
$\mathcal{B}(D_s \to s\bar{s} \to \eta X)$	14.7	2.9	0.2	0.2	1.0	3.7
$\mathcal{B}(D_s \to s\bar{s} \to \eta' X)$	10.3	1.7	0.2	0.1	1.0	0.1
$\mathcal{B}(D_s \to s\bar{s} \to \phi X)$	15.1	1.0	0.0	0.2	0.0	0.0
$\mathcal{B}(D_s \to s\bar{s} \to K\bar{K}X)$	25.4	1.2	0.3	0.6	0.1	0.1
$\mathcal{B}(D_s \to s\bar{s})$	65.6	2.7	0.7	1.0	1.8	3.5
$\mathcal{B}$(Other Annihilation)	21.5	2.8	0.1	0.3	2.0	3.9

A conservative lower bound on $\mathcal{B}$(Other Annihilation) can be obtained by setting $f_1 = f_2 = 0$ and $\mathcal{B}(\text{extra } \eta) = 0$. That gives $\mathcal{B}(\text{Other Annihilation}) = 13.3 \pm 3.0\%$, i.e., $> 9.5\%$ at 90% C.L.. CLEO-c utilizes the measurements of the total kaon yield and the total di-kaon yield to get a measurement of the singly Cabibbo-suppressed rate. The measured branching fraction for $D_s \to$ singly Cabibbo-suppressed is $(7.1 \pm 2.2 \pm 1.3)\%$. The expected branching fraction is $(|V_{\rm us}/V_{\rm ud}|^2 + |V_{\rm cd}/V_{\rm cs}|^2) \times \mathcal{B}(s\bar{s}) \approx \frac{1}{10} \times \mathcal{B}(s\bar{s})$. Taking $\mathcal{B}(s\bar{s})$ from Table 15, get fine agreement between expectations and measurements. CLEO-c also compares the observed pion yields with the minimum pion yields which are computed from the global fit and summarized in Table 16 [30]. The observed yields of π^+, π^-, and π^0 are indeed larger than the corresponding minimum yields of 96.2%, 20.5%, and 46.8%, respectively. Thus, on average, 1/4 of the D_s decays will contain an additional $\pi^+\pi^-$ pair, and 3/4 of the D_s decays will contain an additional π^0 (or 1/2 contain one additional π^0, 1/8 contain two additional π^0's).

10. Other Measurements from CLEO-c

10.1. D_s^+ exclusive hadronic decays involving ω

The inclusive ω yield, $D_s^+ \to \omega X$, has been found substantial: $(6.1 \pm 1.4)\%$ from CLEO-c measurements of D_s^+ inclusive decays [30]. This was very surprising, as the only D_s^+ exclusive decay mode involving ω that had been previously observed is $D_s^+ \to \pi^+\omega$, with a branching fraction of $\mathcal{B}(D_s^+ \to \pi^+\omega) = (0.25 \pm 0.09)\%$ [22]. The presence of certain D_s hadronic decay modes containing an ω could be regarded as evidence for different mechanisms for "weak annihilation" [80]. The decay $D_s^+ \to \pi^+\omega$, forbidden by ordinary annihilation, may proceed through preradiation of the ω, whether via violation of the Okubo-Zweig-Iizuka (OZI) rule [81] or rescattering. The study of ω production in D_s^+ decays is of interest in shedding light on mechanisms

Table 16. The minimum yields of π^+, π^-, and π^0 for each category. Compute the yields of π^+, π^-, and π^0 that come from signal particles. In addition to that, add charged pions to conserve charge. Semileptonic decays have charge conserved via e^+ or μ^+, consequently perform a subtraction to allow for that. (Table from reference, see text.)

Mode	$\mathcal{B}$ (%)	C. C.		Particle Decay			Total Yields		
		π^+	π^-	π^+	π^-	π^0	π^+	π^-	π^0
$D_s^+ \to \eta X$	14.7	14.7	0.0	4.0	4.0	17.7	18.7	4.0	17.7
$D_s^+ \to \eta \bar{s} X$	0.6	0.3	0.0	0.2	0.2	0.7	0.4	0.2	0.7
$D_s^+ \to \eta' X$	10.3	10.3	0.0	9.7	9.7	12.7	20.0	9.7	12.7
$D_s^+ \to \eta' \bar{s} X$	0.4	0.2	0.0	0.4	0.4	0.5	0.6	0.4	0.5
$D_s^+ \to \phi X$	15.1	15.1	0.0	2.4	2.4	2.5	17.5	2.4	2.5
$D_s^+ \to \phi \bar{s} X$	0.6	0.3	0.0	0.1	0.1	0.1	0.4	0.1	0.1
$D_s^+ \to$ Extra ηX	6.0	0.0	0.0	1.6	1.6	7.2	1.6	1.6	7.2
$D_s^+ \to \bar{s} X$ (no η, η')	2.1	1.0	0.0	0.0	0.0	0.0	1.0	0.0	0.0
$D_s^+ \to \bar{s} X, X \to \eta$	1.0	0.5	0.0	0.3	0.3	1.2	0.8	0.3	1.2
$D_s^+ \to \bar{s} X, X \to \eta'$	1.0	0.5	0.0	1.0	1.0	1.3	1.5	1.0	1.3
$D_s^+ \to K_S^0 K_S^0 (K_L^0 K_L^0) X$	3.3	3.3	0.0	0.0	0.0	0.0	3.3	0.0	0.0
$D_s^+ \to K_S^0 K^+ (K_L^0 K^+) X$	11.4	0.0	0.0	0.0	0.0	0.0	0.0	0.0	0.0
$D_s^+ \to K_S^0 K^- (K_L^0 K^-) X$	3.7	7.5	0.0	0.0	0.0	0.0	7.5	0.0	0.0
$D_s^+ \to K^+ K^- (-\phi) X$	7.9	7.9	0.0	0.0	0.0	0.0	7.9	0.0	0.0
$D_s^+ \to K^+ K^+ X$	0.1	0.0	0.1	0.0	0.0	0.0	0.0	0.1	0.0
$D_s^+ \to K^- K^- X$	0.03	0.1	0.0	0.0	0.0	0.0	0.1	0.0	0.0
$D_s^+ \to K_S^0 K_L^0 (-\phi) X$	0.0	0.0	0.0	0.0	0.0	0.0	0.0	0.0	0.0
$D_s^+ \to e^+ (\mu^+) X$	10.7	-10.7	0.0	0.0	0.0	0.0	-10.7	0.0	0.0
$D_s^+ \to \tau^+ \nu$	5.6	0.0	0.0	4.1	0.8	2.9	4.1	0.8	2.9
$D_s^+ \to \mu^+ \nu$	0.6	0.0	0.0	0.0	0.0	0.0	0.0	0.0	0.0
$D_s^+ \to$ Other Annihilation	21.5	21.5	0.0	0.0	0.0	0.0	21.5	0.0	0.0
Minimum Yields							96.2	20.5	46.8
Observed Yields							119.3	43.2	123.4
Additional Yields							23.0	22.7	76.7

of weak decay and their interplay with long-distance (nonperturbative) physics [80].

Using 586 pb^{-1} of data collected at the center-of-mass energy $E_{\rm cm} = 4170$ MeV, CLEO-c has searched for several D_s^+ exclusive hadronic decays involving ω [29]. This analysis utilizes a double-tagging technique, the same as the technique that is used in the D_s^+ inclusive decay analysis [30]. The ω candidates are reconstructed in the $\omega \to \pi^+\pi^-\pi^0$ decay mode. The double-tag (DT) yields are extracted from the $\pi^+\pi^-\pi^0$ invariant mass distribution after requiring that both the tagging D_s and signal D_s invariant masses be in the D_s nominal mass region (20 MeV/c^2 mass window on the tag side and 30 MeV/c^2 mass window on the signal side due to π^0 or η on the signal side). The ω mass signal region is $|M_{\pi^+\pi^-\pi^0} - m_\omega| < 20$ MeV/c^2, while the sideband region is 40 MeV/c^2 $< |M_{\pi^+\pi^-\pi^0} - m_\omega| < 80$ MeV/c^2, where $M_{\pi^+\pi^-\pi^0}$ is the $\pi^+\pi^-\pi^0$ invariant mass and m_ω is the nominal mass of ω [23].

The invariant mass distributions of ω candidates are shown in Fig. 22 [29] and the branching fractions and upper limits are listed in Table 17 [29]. The sum of branching fractions of those four observed modes is (5.4±1.0)%, which accounts for most of

the D_s inclusive ω decays (6.1±1.4)% [30].

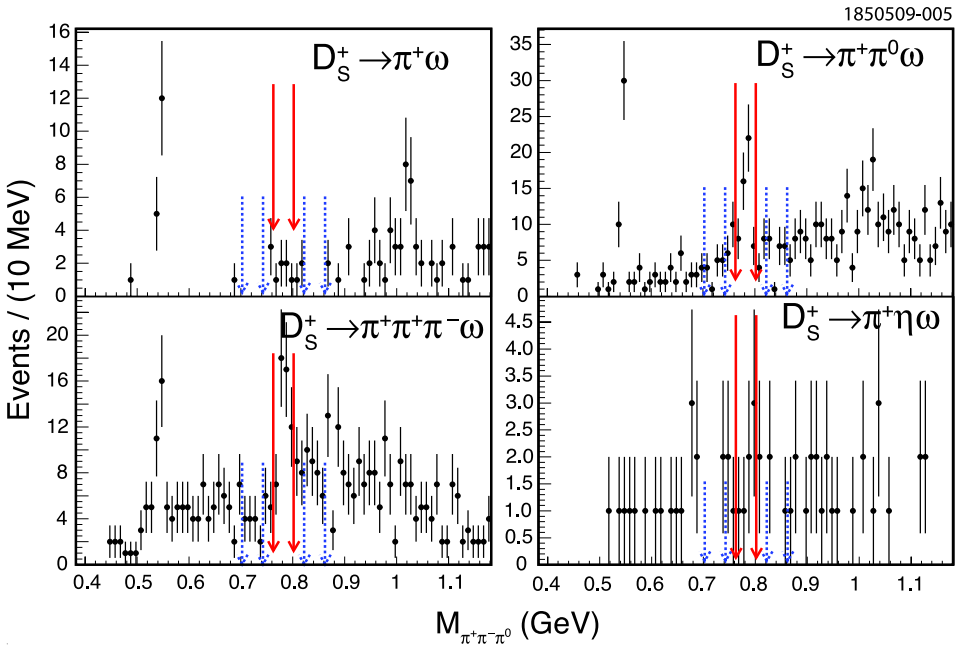

Fig. 22. Invariant mass distributions of ω candidates for the four modes: $D_s^+ \to \pi^+\omega$, $D_s^+ \to \pi^+\pi^0\omega$, $D_s^+ \to \pi^+\pi^+\pi^-\omega$, and $D_s^+ \to \pi^+\eta\omega$. The red solid lines indicate the ω mass signal region and the blue dashed lines indicate the ω mass sideband regions. Peaks from $\eta \to \pi^+\pi^-\pi^0$ and $\phi \to \pi^+\pi^-\pi^0$ are also evident. (Figure from reference, see text.)

Table 17. Branching fractions and upper limits. Uncertainties are statistical and systematic, respectively. (Table from reference, see text.)

Mode	$\mathcal{B}_{\rm mode}(\%)$
$D_s^+ \to \pi^+\omega$	$0.21 \pm 0.09 \pm 0.01$
$D_s^+ \to \pi^+\pi^0\omega$	$2.78 \pm 0.65 \pm 0.25$
$D_s^+ \to \pi^+\pi^+\pi^-\omega$	$1.58 \pm 0.45 \pm 0.09$
$D_s^+ \to \pi^+\eta\omega$	$0.85 \pm 0.54 \pm 0.06$
	< 2.13 (90% CL)
$D_s^+ \to K^+\omega$	< 0.24 (90% CL)
$D_s^+ \to K^+\pi^0\omega$	< 0.82 (90% CL)
$D_s^+ \to K^+\pi^+\pi^-\omega$	< 0.54 (90% CL)
$D_s^+ \to K^+\eta\omega$	< 0.79 (90% CL)

10.2. *Determination of relative strong phase between D^0 and $\bar{D}^0$*

Threshold production of $D\bar{D}$ pairs can be explored to understand the phase structure of hadronic decay amplitudes of D^0 mesons. Quantum correlation in the coherent $\psi(3770) \to D^0\bar{D}^0$ decay provides direct sensitivity to the relative strong phase difference $\Delta\delta_D$ between D^0 and $\bar{D}^0$ decaying to a common final state. Using 818 pb^{-1} data collected at the $\psi(3770)$ resonance, CLEO-c published the first measurement of the relative strong phase differences between $D^0 \to K^0_S\pi^+\pi^-$ and $\bar{D}^0 \to K^0_S\pi^+\pi^-$, which are important input to the determination of the Cabibbo-Kobayashi-Maskawa angle γ/ϕ_3 in $B^- \to D^0(\bar{D}^0)K^-$ [82]. The measured values of c_i and s_i (the cosine and sine of the strong phase difference) for $D^0 \to K^0_S\pi^+\pi^-$ are shown in Fig. 23 [82]. They are in good agreement with the predicted values [83]. A more comprehensive review of the analysis of quantum correlated $D\bar{D}$ decays can be found in Ref. [84].

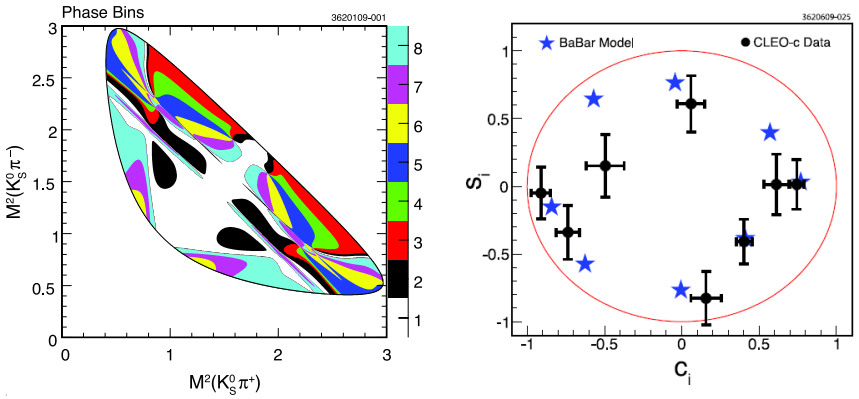

Fig. 23. Phase binning of $D^0 \to K^0_S\pi^+\pi^-$ Dalitz plot (left); results for c_i and s_i (right). Error bars indicate the measured values; stars indicate the predicted values from the BABAR model. (Figure from reference, see text.)

10.3. *Observation of the baryonic decay $D_s^+ \to p\bar{n}$*

The process $D_s^+ \to p\bar{n}$ is the only kinematically allowed decay of a ground state charmed meson to baryons. This decay is quite interesting because the flavors of all valence quarks that constitute the initial state ($c\bar{s}$) differ from the flavors of the final-state quarks composing the $p\bar{n}$ pair. Thus, it is quite tempting to declare that the transition $D_s^+ \to p\bar{n}$ proceeds only via the weak annihilation graph [85,86,87,88].

The first observation of the decay $D_s^+ \to p\bar{n}$ has been made by CLEO-c using 325 pb^{-1} data taken at a center-of-mass energy of 4170 MeV [89]. CLEO-c reconstructs the anti-neutron from the missing mass with virtually no background. The results are shown in Fig. 24 [89]. Thirteen events and no background yields a branch-

ing fraction [89]

$$\mathcal{B}(D_s^+ \to p\bar{n}) = \left(1.30 \pm 0.36^{+0.12}_{-0.16}\right) \times 10^{-3}.$$

This decay mode is dominated by long-distance effects as those shown in Fig. 25 [88], and has been estimated [88] as $\mathcal{B}(D_s^+ \to p\bar{n}) \approx \left(0.8^{+2.4}_{-0.6}\right) \times 10^{-3}$ in agreement with CLEO-c's observation. Short-distance contributions from the annihilation diagram are about 3 orders of magnitude smaller.

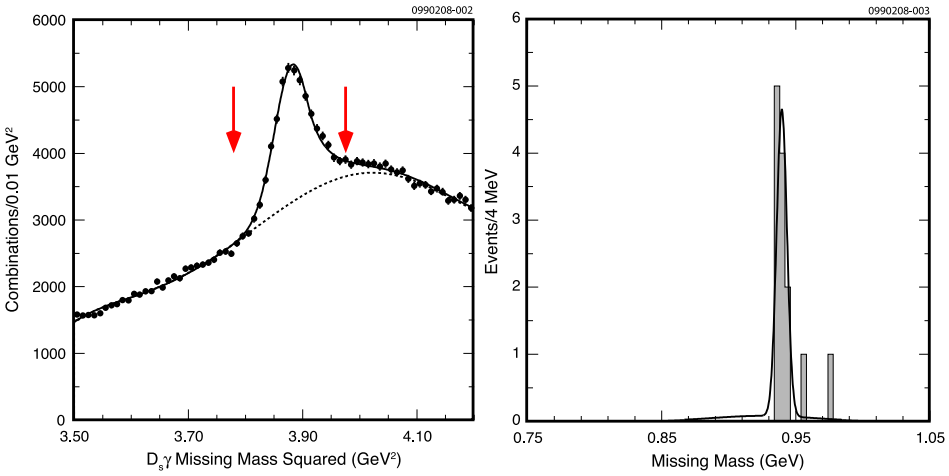

Fig. 24. Observation of $D_s^+ \to p\bar{n}$ at CLEO-c. Left: missing mass squared of tag $D_s\gamma$ combination, showing peak at $m^2_{D_s}$ for true $D_s^{*\pm}D_s^{\mp}$ events. Candidates within the red arrows are then investigated for $D_s^+ \to p\bar{n}$ candidates. Right: missing mass opposite $D_s\gamma p$ system showing peak at m_n. The solid line shows the expected signal distribution. (Figure from reference, see text.)

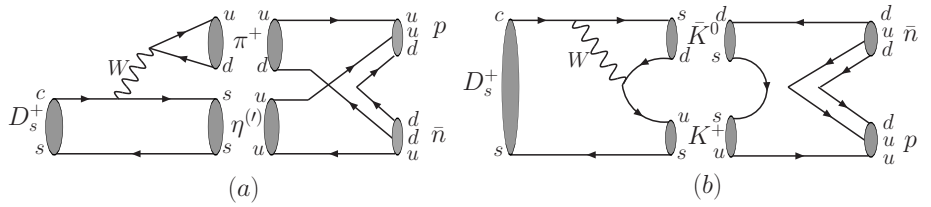

Fig. 25. Long-distance contributions to $D_s^+ \to p\bar{n}$ via final-state rescattering of (a) the W-emission amplitude of $D_s^+ \to \pi^+\eta^{(\prime)}$ and (b) the color-suppressed amplitude of $D_s^+ \to K^+\bar{K}^0$. Both diagrams have the same topology as W-annihilation. (Figure from reference, see text.)

10.4. *Search for $D^0 \to \bar{p}e^+$ and $D^0 \to pe^-$*

Using 281 pb^{-1} data collected at the $\psi(3770)$ resonance, CLEO-c has searched for simultaneous baryon and lepton number violating decays of the D^0 meson and found no significant signals. The branching fraction upper limits are $\mathcal{B}(D^0 \to \bar{p}e^+) < 1.1 \times 10^{-5}$ and $\mathcal{B}(D^0 \to pe^-) < 1.0 \times 10^{-5}$ at 90% confidence level [90].

10.5. *Precision determination of the D^0 Mass*

A precision measurement of the D^0 meson mass has been made by CLEO-c using same 281 pb^{-1} data collected at the $\psi(3770)$ resonance [91]. The exclusive decay $D^0 \to K_S\phi$ has been used to obtain $M(D^0) = 1864.847 \pm 0.150 \pm 0.095$ MeV/c^2 [91], which corresponds to $M(D^0\bar{D}^{*0}) = 3871.81 \pm 0.36$ MeV/c^2, and leads to a well-constrained determination of the binding energy of the proposed $D^0\bar{D}^{*0}$ molecule $X(3872)$ [92,93,94,95], as $E_b = 0.6 \pm 0.6$ MeV.

10.6. *Rare and forbidden decays $D^+_{(s)} \to h^\pm e^\mp e^+$*

A previous search for decays $D^+ \to h^\pm e^\mp e^+$ using 281 pb^{-1} data collected at the $\psi(3770)$ resonance has been published by CLEO-c [96]. Later CLEO-c updated and extended this search for flavor-changing neutral current decays and lepton-number-violating decays of D^+ and D_s^+ mesons to final states of the form $h^\pm e^\mp e^+$, where h is either π or K, using the complete samples of CLEO-c open charm data, 818 pb^{-1} at $E_{\rm cm} = 3774$ MeV and 602 pb^{-1} at $E_{\rm cm} = 4170$ MeV [97]. These decays probe flavor-changing neutral currents (FCNC), in $D^+ \to \pi^+e^+e^-$ and $D_s^+ \to K^+e^+e^-$, and lepton number violations (LNV), in $D^+ \to h^-e^+e^+$ and $D_s^+ \to h^-e^+e^+$. These decays are either highly suppressed or forbidden in the standard model (SM), but can be significantly enhanced by some non-SM physics scenarios [98,99,100,101,102,103]. Scatterplots of ΔE vs $\Delta M_{\rm bc}$ and $\Delta M(D_s^+)$ vs $\Delta M_{\rm recoil}(D_s^+)$ for signal candidates with all background suppressions applied are shown in Figs. 26 [97] and 27 [97]. No evidence of signals is found except for $\phi(e^+e^-)\pi^+$ channels. The 90% confidence level upper limits on the branching fractions based on *Poisson processes with background* [104] (e.g. Section 28.6.4 *Poisson processes with background* therein) are summarized in Table 18 [97].

11. Conclusions and Outlook

CLEO-c has performed sophisticated studies of hadronic D decays with the large dataset collected at the charm threshold in the last few years. These results have reduced branching fraction uncertainties by factors of 2 to 4, provided the discovery of many new decay channels and first measurements of strong interaction phases between two body decays, improved our understanding of decay dynamics, and contributed important input to the analysis of B decays. The CLEO-c's dataset will continue to be analysed, and the high-luminosity BES III experiment has already started taking data. The prospects for charm physics are bright.

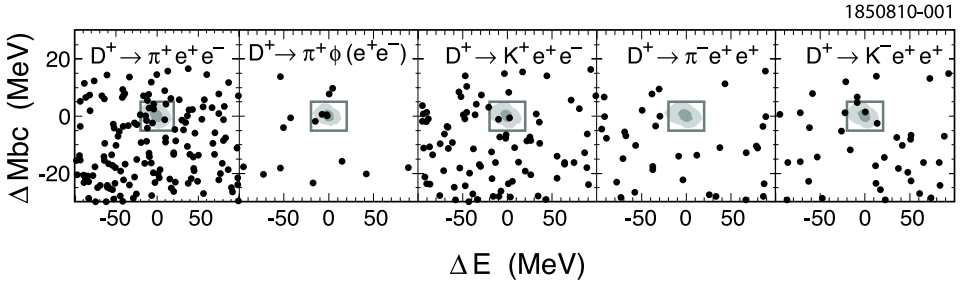

Fig. 26. Scatterplots of $\Delta M_{\rm bc}$ vs ΔE. The two contours for each mode enclose regions determined with signal MC simulation to contain 50% and 85% of signal events, respectively. The signal region, defined by $(\Delta E, \Delta M_{\rm bc}) = (\pm 20\,{\rm MeV}, \pm 5\,{\rm MeV})$, is shown as a box. (Figure from reference, see text.)

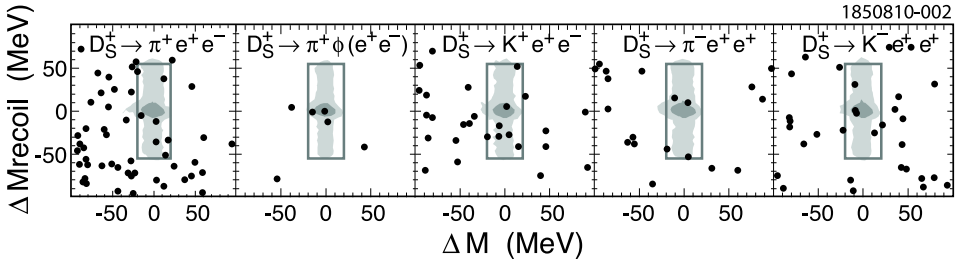

Fig. 27. Scatterplots of $\Delta M_{\rm recoil}$ vs ΔM. The two contours for each mode enclose regions determined with signal MC simulation to contain 40% and 85% of signal events, respectively. The signal region, defined by $(\Delta M, \Delta M_{\rm recoil}) = (\pm 20\,{\rm MeV}, \pm 55\,{\rm MeV})$, is shown as a box. (Figure from reference, see text.)

12. Acknowledgments

The author would like to thank his colleagues for helpful conversations and discussions, especially Ed. Thorndike, for his careful reading of the manuscript and useful comments, and the CLEO Calibration for the use of the many results and figures.

References

1. J. J. Aubert *et al.* [E598 Collaboration], Phys. Rev. Lett. **33**, 1404 (1974).
2. J. E. Augustin *et al.* [SLAC-SP-017 Collaboration], Phys. Rev. Lett. **33**, 1406 (1974).
3. G. Goldhaber *et al.*, Phys. Rev. Lett. **37**, 255 (1976).
4. I. Peruzzi *et al.*, Phys. Rev. Lett. **37**, 569 (1976).
5. A. Chen *et al.* [CLEO Collaboration], Phys. Rev. Lett. **51**, 634 (1983).
6. G. Cavoto *et al.*, arXiv:hep-ph/0603019 (2006).
7. B. Aubert *et al.* [BABAR Collaboration], Phys. Rev. D **71**, 032005 (2005)
8. A. Giri, Y. Grossman, A. Soffer and J. Zupan, Phys. Rev. D **68**, 054018 (2003)
9. K. Abe *et al.* [BELLE Collaboration], Phys. Rev. Lett. **99**, 131803 (2007)
10. A. Ryd and A. A. Petrov, arXiv:0910.1265 [hep-ph].
11. M. Artuso, B. Meadows and A. A. Petrov, Ann. Rev. Nucl. Part. Sci. **58**, 249 (2008)

Table 18. Upper limits on branching fractions of D^+ and $D_s^+ \to h^\pm e^\mp e^+$ at the 90% confidence level for a Poisson process, where N is the number of D^+ (or D_s^+) produced in data, ϵ is the signal efficiency, $N_{\rm exp}$ is the number of expected background, $N_{\rm obs}$ is the number of signal candidates, $\mathcal{C}(N_{\rm obs}|N_{\rm exp})$ is the 90% confidence coefficient upper limit on the observed events given the expected background, and $\mathcal{B}$ is the branching fraction or upper limit of the branching fraction at 90% confidence level. The upper limits have been increased to account for systematic uncertainties. (Table from reference, see text.)

Channel	N	ϵ (%)	$N_{\rm exp}$	$N_{\rm obs}$	$\mathcal{C}(N_{\rm obs}\|N_{\rm exp})$	$\mathcal{B}$
$D^+ \to \pi^+e^+e^-$	4.76×10^6	33.9	5.7	9	9.3	$< 5.9\times10^{-6}$
$D^+ \to \pi^-e^+e^+$	4.76×10^6	43.5	1.3	0	2.3	$< 1.1\times10^{-6}$
$D^+ \to K^+e^+e^-$	4.76×10^6	23.1	4.9	2	3.2	$< 3.0\times10^{-6}$
$D^+ \to K^-e^+e^+$	4.76×10^6	35.3	1.2	3	5.8	$< 3.5\times10^{-6}$
$D^+ \to \pi^+\phi(e^+e^-)$	4.76×10^6	46.2	0.3	4		$(1.7^{+1.4}_{-0.9}\pm0.1)\times10^{-6}$
					7.9	$< 3.7\times10^{-6}$
$D_s^+ \to \pi^+e^+e^-$	1.10×10^6	24.3	6.7	6	5.6	$< 2.2\times10^{-5}$
$D_s^+ \to \pi^-e^+e^+$	1.10×10^6	33.4	2.2	4	6.2	$< 1.8\times10^{-5}$
$D_s^+ \to K^+e^+e^-$	1.10×10^6	17.3	3.0	7	9.3	$< 5.2\times10^{-5}$
$D_s^+ \to K^-e^+e^+$	1.10×10^6	27.7	4.1	4	5.0	$< 1.7\times10^{-5}$
$D_s^+ \to \pi^+\phi(e^+e^-)$	1.10×10^6	33.9	0.7	3		$(0.6^{+0.8}_{-0.4}\pm0.1)\times10^{-5}$
					6.2	$< 1.8\times10^{-5}$

12. E. H. Thorndike [CLEO Collaboration], Int. J. Mod. Phys. A **23**, 3183 (2008).
13. Y. Kubota *et al.* [CLEO Collaboration], Nucl. Instrum. Meth. A **320**, 66 (1992).
14. D. Peterson *et al.*, Nucl. Instrum. Meth. A **478**, 142 (2002).
15. M. Artuso *et al.*, Nucl. Instrum. Meth. A **554**, 147 (2005)
16. S. Dobbs *et al.* [CLEO Collaboration], Phys. Rev. D **76**, 112001 (2007)
17. R. Brun *et al.*, GEANT 3.21, CERN Program Library Long Writeup W5013 (unpublished) 1993.
18. D.J. Lange, Nucl. Instrum. Methods Phys. Res., Sec. A **462**, 152 (2001).
19. E. Barberio and Z. Wąs, Comput. Phys. Commun. **79**, 291 (1994).
20. D. Cronin-Hennessy *et al.* [CLEO Collaboration], Phys. Rev. D **80**, 072001 (2009)
21. W. M. Yao *et al.* [Particle Data Group], J. Phys. G **33**, 1 (2006).
22. C. Amsler *et al.* [Particle Data Group], Phys. Lett. B **667**, 1 (2008).
23. K. Nakamura *et al.* [Particle Data Group], J. Phys. G **37**, 075021 (2010).
24. B. Aubert *et al.* [BABAR Collaboration], Phys. Rev. D **72**, 091101 (2005)
25. R. M. Baltrusaitis *et al.* [MARK-III Collaboration], Phys. Rev. Lett. **56**, 2140 (1986).
26. J. Adler *et al.* [MARK-III Collaboration], Phys. Rev. Lett. **60**, 89 (1988).
27. S. A. Dytman *et al.* [CLEO Collaboration], Phys. Rev. D **74**, 071102 (2006)
28. G. S. Adams *et al.* [CLEO Collaboration], Phys. Rev. Lett. **99**, 191805 (2007)
29. J. Y. Ge *et al.* [CLEO Collaboration], Phys. Rev. D **80**, 051102 (2009)
30. S. Dobbs *et al.* [CLEO Collaboration], Phys. Rev. D **79**, 112008 (2009)
31. H. Mendez *et al.* [CLEO Collaboration], Phys. Rev. D **81**, 052013 (2010)
32. F. Buccella, M. Lusignoli, G. Miele, A. Pugliese and P. Santorelli, Phys. Rev. D **51**, 3478 (1995)
33. M. Bauer, B. Stech and M. Wirbel, Z. Phys. C **34**, 103 (1987).
34. A. J. Buras, J. M. Gerard and R. Ruckl, Nucl. Phys. B **268**, 16 (1986).
35. B. Blok and M. A. Shifman, Nucl. Phys. B **399**, 441 (1993) [arXiv:hep-ph/9207236].
36. A. F. Falk, Y. Nir and A. A. Petrov, JHEP **9912**, 019 (1999)

37. M. J. Savage, Phys. Lett. B **257**, 414 (1991).
38. M. Gronau, O. F. Hernandez, D. London and J. L. Rosner, Phys. Rev. D **50**, 4529 (1994)
39. J. L. Rosner, Phys. Rev. D **60**, 114026 (1999)
40. J. D. Richman and P. R. Burchat, Rev. Mod. Phys. **67**, 893 (1995)
41. Q. He *et al.* [CLEO Collaboration], Phys. Rev. Lett. **95**, 121801 (2005)
42. H. Albrecht *et al.* [ARGUS Collaboration], Phys. Lett. B **241**, 278 (1990).
43. W. M. Sun, Nucl. Instrum. Meth. A **556**, 325 (2006)
44. B. Aubert *et al.* [BABAR Collaboration], Phys. Rev. Lett. **100**, 051802 (2008)
45. S. Bianco, F. L. Fabbri, D. Benson and I. Bigi, Riv. Nuovo Cim. **26N7**, 1 (2003)
46. M. Ablikim *et al.* [BES Collaboration], Phys. Rev. Lett. **97**, 121801 (2006)
47. D. Besson *et al.* [CLEO Collaboration], Phys. Rev. Lett. **96**, 092002 (2006)
48. D. Besson *et al.* [CLEO Collaboration], Phys. Rev. Lett. **104**, 159901 (2010)
49. J. P. Alexander *et al.* [CLEO Collaboration], Phys. Rev. Lett. **100**, 161804 (2008)
50. A. A. Petrov, Phys. Rev. D **69**, 111901 (2004)
51. F. Buccella, M. Lusignoli, G. Mangano, G. Miele, A. Pugliese and P. Santorelli, Phys. Lett. B **302**, 319 (1993)
52. Y. Grossman, A. L. Kagan and Y. Nir, Phys. Rev. D **75**, 036008 (2007)
53. L. L. Chau and H. Y. Cheng, Phys. Lett. B **222**, 285 (1989).
54. A. N. Kamal and R. C. Verma, Phys. Rev. D **35**, 3515 (1987) [Erratum-ibid. D **36**, 3527 (1987)] [Phys. Rev. D **36**, 3527 (1987)].
55. E. Golowich and A. A. Petrov, Phys. Lett. B **427**, 172 (1998)
56. L. L. Chau and H. Y. Cheng, Phys. Lett. B **280**, 281 (1992).
57. P. Rubin *et al.* [CLEO Collaboration], Phys. Rev. Lett. **96**, 081802 (2006)
58. S. Eidelman *et al.* [Particle Data Group], Phys. Lett. B **592**, 1 (2004).
59. M. Artuso *et al.* [CLEO Collaboration], Phys. Rev. D **77**, 092003 (2008)
60. G. Bonvicini *et al.* [CLEO Collaboration], Phys. Rev. D **77**, 091106 (2008)
61. B. Aubert *et al.* [BABAR Collaboration], Phys. Rev. D **74**, 011107 (2006)
62. I. I. Y. Bigi and H. Yamamoto, Phys. Lett. B **349**, 363 (1995)
63. J. L. Rosner, Phys. Rev. D **74**, 057502 (2006)
64. D. N. Gao, Phys. Lett. B **645**, 59 (2007)
65. Q. He *et al.* [CLEO Collaboration], Phys. Rev. Lett. **100**, 091801 (2008)
66. B. Bhattacharya and J. L. Rosner, Phys. Rev. D **77**, 114020 (2008)
67. B. Bhattacharya and J. L. Rosner, Phys. Rev. D **81**, 014026 (2010)
68. B. R. Ko *et al.* [Belle collaboration], Phys. Rev. Lett. **104**, 181602 (2010)
69. L. L. Chau, Phys. Rept. **95**, 1 (1983).
70. L. L. Chau and H. Y. Cheng, Phys. Rev. Lett. **56**, 1655 (1986).
71. C. W. Chiang, Z. Luo and J. L. Rosner, Phys. Rev. D **67**, 014001 (2003)
72. H. Y. Cheng and C. W. Chiang, Phys. Rev. D **81**, 074021 (2010)
73. J. Rademacker [CLEO-c Collaboration], arXiv:1002.2896 [hep-ex].
74. G. S. Huang *et al.* [CLEO Collaboration], Phys. Rev. D **74**, 112005 (2006)
75. D. G. Cassel, *In the Proceedings of International Conference on Heavy Quarks and Leptons (HQL 06), Munich, Germany, 16-20 Oct 2006, pp 026* [arXiv:hep-ex/0702021].
76. M. Gronau and J. L. Rosner, Phys. Rev. D **79**, 074022 (2009)
77. E. Fermi, Phys. Rev. **92**, 452 (1953); **93**, 1434(E) (1954); K. M. Watson, Phys. Rev. **85**, 852 (1952); I. Smushkevich, Dokl. Akad. Nauk SSSR **103**, 235 (1955); A. Pais, Ann. Phys. (N.Y.) **9**, 548 (1960); **22**, 274 (1963); M. Peshkin, Phys. Rev. **121**, 636 (1961).
78. M. Peshkin and J. L. Rosner, Nucl. Phys. B **122**, 144 (1977).

79. C. Quigg and J. L. Rosner, Phys. Rev. D **17**, 239 (1978).
80. M. Gronau and J. L. Rosner, Phys. Rev. D **79**, 074006 (2009)
81. S. Okubo, Phys. Lett. **5**, 165 (1963); G. Zweig, CERN Report No. 8419/TH–412 (1964); J. Iizuka, Prog. Theor. Phys. Suppl. **37**, 21 (1966).
82. R. A. Briere *et al.* [CLEO Collaboration], Phys. Rev. D **80**, 032002 (2009)
83. B. Aubert *et al.* [BABAR Collaboration], Phys. Rev. Lett. **95**, 121802 (2005)
84. G. Wilkinson, arXiv:0910.0401 [hep-ex].
85. X. Y. Pham, Phys. Lett. B **94**, 231 (1980).
86. X. Y. Pham, Phys. Rev. Lett. **45**, 1663 (1980).
87. I. Bediaga and E. Predazzi, Phys. Lett. B **275**, 161 (1992).
88. C. H. Chen, H. Y. Cheng and Y. K. Hsiao, Phys. Lett. B **663**, 326 (2008)
89. S. B. Athar *et al.* [CLEO Collaboration], Phys. Rev. Lett. **100**, 181802 (2008)
90. P. Rubin *et al.* [CLEO Collaboration], Phys. Rev. D **79**, 097101 (2009)
91. C. Cawlfield *et al.* [CLEO Collaboration], Phys. Rev. Lett. **98**, 092002 (2007)
92. S. K. Choi *et al.* [Belle Collaboration], Phys. Rev. Lett. **91**, 262001 (2003)
93. D. E. Acosta *et al.* [CDF II Collaboration], Phys. Rev. Lett. **93**, 072001 (2004)
94. V. M. Abazov *et al.* [D0 Collaboration], Phys. Rev. Lett. **93**, 162002 (2004)
95. B. Aubert *et al.* [BABAR Collaboration], Phys. Rev. D **71**, 071103 (2005)
96. Q. He *et al.* [CLEO Collaboration], Phys. Rev. Lett. **95**, 221802 (2005)
97. P. Rubin *et al.* [CLEO Collaboration], Phys. Rev. D **82**, 092007 (2010)
98. G. Burdman, E. Golowich, J. Hewett and S. Pakvasa, Phys. Rev. D **66**, 014009 (2002).
99. S. Fajfer, S. Prelovsek and P. Singer, Phys. Rev. D **64**, 114009 (2001).
100. S. Fajfer and S. Prelovsek, Phys. Rev. D **73**, 054026 (2006).
101. S. Fajfer, N. Kosnik and S. Prelovsek, Phys. Rev. D **76**, 074010 (2007).
102. A. Ali, A. V. Borisov and N. B. Zamorin, Eur. Phys. J. C **21**, 123 (2001).
103. A. Atre, T. Han, S. Pascoli and B. Zhang, JHEP **0905**, 030 (2009).
104. R. M. Barnett *et al.* [Particle Data Group], Phys. Rev. D **54**, 1 (1996).